

Full-shape cosmology analysis of SDSS-III BOSS galaxy power spectrum using emulator-based halo model: a 5% determination of σ_8

Yosuke Kobayashi^{1,2,*}, Takahiro Nishimichi^{3,2}, Masahiro Takada^{2,†} and Hironao Miyatake^{4,2}

¹ *Department of Astronomy/Steward Observatory, University of Arizona,
933 North Cherry Avenue, Tucson, AZ 85721-0065, USA*

² *Kavli Institute for the Physics and Mathematics of the Universe (WPI),
The University of Tokyo Institutes for Advanced Study (UTIAS),
The University of Tokyo, Chiba 277-8583, Japan*

³ *Center for Gravitational Physics, Yukawa Institute for Theoretical Physics, Kyoto University, Kyoto 606-8502, Japan*

⁴ *Kobayashi-Maskawa Institute for the Origin of Particles and the
Universe (KMI), Nagoya University, Nagoya, 464-8602, Japan*

We present the results obtained from the full-shape cosmology analysis of the redshift-space power spectra for 4 galaxy samples of the SDSS-III BOSS DR12 galaxy catalog over $0.2 < z < 0.75$. For the theoretical template, we use an emulator that was built from an ensemble set of N -body simulations, which enables fast and accurate computation of the redshift-space power spectrum of “halos”. Combining with the halo occupation distribution to model the halo-galaxy connection, we can compute the redshift-space power spectrum of BOSS-like galaxies in less than a CPU second, for an input model under flat Λ CDM cosmology. In our cosmology inference, we use the monopole, quadrupole and hexadecapole moments of the redshift-space power spectrum and include 7 nuisance parameters, with broad priors, to model uncertainties in the halo-galaxy connection for each galaxy sample, but do not use any information on the abundance of galaxies. We demonstrate a validation of our analysis pipeline using the mock catalogs of BOSS-like galaxies, generated using different recipes of the halo-galaxy connection and including the assembly bias effect. Assuming weak priors on cosmological parameters, except for the BBN prior on $\Omega_b h^2$ and the CMB prior on n_s , we show that our model well reproduces the BOSS power spectra. Including the power spectrum information up to $k_{\text{max}} = 0.25 h \text{ Mpc}^{-1}$, we find $\Omega_m = 0.300 \pm 0.011$, $H_0 = 68.35^{+1.21}_{-1.39} \text{ km s}^{-1} \text{ Mpc}^{-1}$, and $\sigma_8 = 0.742^{+0.035}_{-0.036}$, for the mode and 68% credible interval, after marginalization over nuisance parameters including the halo-galaxy connection parameters. We find little improvement in the cosmological parameters beyond a maximum wavelength $k_{\text{max}} \simeq 0.2 h \text{ Mpc}^{-1}$ due to the shot noise domination and marginalization of the halo-galaxy connection parameters. Our results show a nice agreement with the *Planck* CMB results for Ω_m and H_0 , but indicate a slight tension for σ_8 .

I. INTRODUCTION

The three-dimensional distribution of galaxies, measured from wide-area spectroscopic surveys of galaxies, is a powerful probe of cosmology, *e.g.*, for constraining cosmological parameters such as parameters characterizing the nature of dark energy and for testing gravity theory on cosmological scales [1–7]. To attain the fundamental cosmology, there are various exiting, ongoing and planned galaxy redshift surveys: the SDSS-III Baryon Oscillation Spectroscopic Survey (BOSS; [8]), the SDSS-IV extended Baryon Oscillation Spectroscopic Survey (eBOSS; [9]), the Subaru Prime Focus Spectrograph (PFS; [10]), the Dark Energy Spectroscopic Instrument (DESI; [11]), the ESA *Euclid* satellite mission [12], and the NASA Nancy Grace Roman Space Telescope [13].

The galaxy distribution observed by spectroscopic surveys is modulated by the Doppler effect due to the line-of-sight peculiar velocities of galaxies, and exhibits characteristic anisotropies, called the redshift-space distortion (RSD) [14–16]. The RSD effect is useful to improve cos-

mological constraints by breaking degeneracies between the cosmological parameters and uncertainties in galaxy bias relative to the underlying matter distribution [17]. In addition, since the RSD effect is a gravitational effect, it can be used, if precisely measured, to probe the strength of gravitational field in large-scale structure, which can be in turn used to test gravity theory on cosmological scales.

In order to exploit the full information from galaxy redshift surveys, we need a sufficiently accurate theoretical template that enables a high-fidelity comparison with the measured clustering statistics of galaxies to obtain a robust estimate of cosmological parameters. The linear theory of cosmological fluctuations, which has been in a remarkable success in CMB analyses, ceases to be accurate at $k \gtrsim 0.1 h \text{ Mpc}^{-1}$ due to nonlinear effects of structure formation [17]. The standard approach to tackle this difficulty has been analytic prescriptions based on the perturbation theory of large-scale structure [18, 19]. This approach describes the distribution of galaxies in terms of a series expansion of both the matter density and velocity fields with a set of free coefficients/terms including bias parameters, under the single-stream approximation [20, 21]. A further refined model consistently separating short-scale physics including the galaxy bias from large-scale dynamics of interest, so-called Effic-

* yosukekobayashi@email.arizona.edu

† masahiro.takada@ipmu.jp

tive Field Theory of Large-Scale Structure (EFTofLSS), has also been developed [22]. These models have been applied to actual datasets to obtain cosmological constraints [5, 23–27]. While these perturbation theory-based templates give useful predictions at linear and quasi-nonlinear scales up to $k \sim 0.2 h \text{ Mpc}^{-1}$, application of these models to even smaller scales is still disturbed by even higher-order contributions of both the density and velocity fields as well as non-perturbative effects arising from the dynamics beyond shell crossing, *i.e.*, formation of galaxies (or dark matter halos) [*e.g.*, 28–34]. Consequently, the cosmological analysis of the galaxy power spectrum has been typically limited to the wave number $k \lesssim 0.15 - 0.2 h \text{ Mpc}^{-1}$, depending on the redshift and the accuracy of the model required to meet the statistical precision of data [24, 25, 35]. In other words, the clustering information on the higher- k scales does not seem practical for cosmology in this method, because the information is used to basically constrain higher-order bias parameters and other nuisance parameters that need to be introduced for the theoretical consistency of models.

As an alternative approach, in this paper we use a simulation-based theoretical template, the *emulator*, which enables fast and accurate computation of the redshift-space power spectrum of “halos” in the flat Λ CDM framework, developed in our previous paper [36]. Dark matter halos are the places where galaxies likely form. It is relatively straightforward to accurately simulate the formation and evolution processes of halos using N -body simulations and then have an accurate prediction of their clustering properties including the redshift-space power spectrum [19, 37]. Kobayashi *et al.* [36] developed an emulator by training a feed-forward neural network with a dataset of the redshift-space power spectra of halos measured from halo catalogs in an ensemble set of N -body simulations for 80 models within flat w CDM framework in the DARK QUEST campaign [38]. The emulator was validated using the test dataset consisting of 20 cosmological models that are not in training, and it was shown that the power spectra are sufficiently accurate up to $k = 0.6 h \text{ Mpc}^{-1}$. The emulator includes all the non-perturbative, nonlinear effects relevant to the formation and evolution of halos: nonlinear clustering, nonlinear RSD, nonlinear bias of halos, and halo exclusion effect. By combining with a halo occupation distribution (HOD) model [39–44], the emulator enables to compute the redshift-space power spectrum of galaxies in less than a CPU second on a typical recent laptop computer. Thus, the emulator allows for cosmological parameter inference of the galaxy power spectrum in a multi-dimensional parameter space. Such an emulator-based method is equivalent to estimating cosmological parameters from comparison of the observed power spectrum with mock spectra from simulated galaxy catalogs generated from costly high-resolution N -body simulations with varying cosmological models.

Hence, the purpose of this paper is to perform a cosmological analysis of the redshift-space galaxy power spec-

trum measured from the public BOSS DR12 large-scale structure catalog over $0.2 < z < 0.75$ [45], using the aforementioned emulator. In doing this, we analyze the “full-shape” information in the monopole, quadrupole and hexadecapole moments of the redshift-space power spectra, beyond the traditional approach to extract only geometrical information through the features of baryon acoustic oscillations (BAO) and the anisotropy originating from RSD. We first show a series of validation checks of our method to ensure unbiased cosmological inference beyond the accuracy assessment of the emulator at the halo power spectrum level already presented in our previous paper. We apply the full analysis pipeline to mock signals of the galaxy power spectrum measured from the galaxy mock catalogs and then check whether our method can recover the cosmological parameters to within the statistical errors. For this validation, we use the mock catalogs generated using different recipes of halo-galaxy connection from our fiducial HOD model [also see 35, for similar analyses but with different observables] and also use mock catalogs including the assembly bias effect that is one of the most dangerous, physical systematic effects in the halo model approach. We then apply the analysis method to the galaxy power spectra measured from the BOSS catalog under the flat Λ CDM cosmology. In doing this, we employ weak priors on the cosmological parameters, except for the BBN prior on $\Omega_b h^2$ [46] and the CMB prior on n_s [47], employ very broad priors for the halo-galaxy connection parameters, and then estimate the cosmological parameters including marginalization over uncertainties in the nuisance parameters. We also compare our cosmological constraints with the EFTofLSS results [26] and the *Planck* 2018 cosmological results [47].

The structure of this paper is as follows. In Sec. II we will describe details of the galaxy samples constructed from the BOSS catalog and procedures of the redshift-space power spectrum measurements and the covariance estimation. In Sec. III we will describe details of the emulator-based halo model as the theoretical template and then the parameters and priors used in the cosmology analysis. In Sec. IV we show the main results of this paper: the cosmological parameters for the flat Λ CDM model. In Sec. V we give discussion on possible residual systematic effects in the data and the theoretical template. Sec. VI is devoted to the conclusion.

II. BOSS GALAXY CATALOG, POWER SPECTRUM AND COVARIANCE

We measure by ourselves the monopole, quadrupole, and hexadecapole moments of the redshift-space power spectrum up to a higher k_{max} than the publicly available spectrum, from each sample constructed from the public BOSS galaxy catalog. For the measurement, we employ a fast Fourier Transform (FFT)-based estimator of power spectrum multipoles, following the method in Ref. [48]. In this section, we describe our measurement method.

A. Power spectrum measurement

Throughout this work, we use the publicly available large-scale structure catalog named CMASSLOWZTOT, the BOSS DR12 public large-scale structure catalog that is available from <https://data.sdss.org/sas/dr12/booss/lss/>. This catalog consists of two galaxy samples that are selected based on different color and magnitude cuts, LOWZ and CMASS samples, including the weights (see Ref. [49] for the detailed description of the catalog creation). For the random particles, we use the `random0` catalog for CMASSLOWZTOT samples, which contains the larger number of random particles than that of galaxies by a factor of ~ 50 . We split the two galaxy samples into non-overlapping redshift bins, which we denote as low- z ($0.2 < z < 0.5$) and high- z ($0.5 < z < 0.75$) samples, respectively, following Ref. [26].

Table I gives details of the galaxy samples in each redshift bin. N_{gal} is the unweighted number of galaxies, *i.e.*, a naive count of galaxies listed in the catalog. In reality, each galaxy is assigned a completeness weight to take into account the correction of observational systematics. In the BOSS galaxy catalogs, the completeness weight consists of three types of weights [49]:

$$w_c = w_{\text{sys}}(w_{\text{fc}} + w_{\text{rf}} - 1), \quad (1)$$

where w_{fc} is the fiber collision weight, w_{rf} is the redshift failure weight, and w_{sys} is the systematics weight which is estimated from the stellar density and seeing systematics in each field where each galaxy resides. In Table I we also give the weighted number of galaxies that is estimated by $N_{\text{gal}}^c = \sum_{i=1}^{N_{\text{gal}}} w_{c,i}$. Aside from the completeness weight, each galaxy is also assigned the so-called Feldman-Kaiser-Peacock (FKP) weight [50] to improve the signal-to-noise ratio in the measurement of galaxy power spectra. Following the usual setting, we adopt the FKP weight in the form of

$$w_{\text{FKP},i} = \frac{1}{1 + \bar{n}_g(z_i)P_0}, \quad (2)$$

where z_i is the spectroscopic redshift of the i -th galaxy, $\bar{n}_g(z_i)$ is the mean galaxy number density at redshift z_i , and we adopt $P_0 = 10^4 h^{-3} \text{Mpc}^3$.

To compute the theoretical model of the galaxy power spectrum, we use a single effective redshift z_{eff} for each redshift bin. We define it as the weighted mean redshift over the galaxy sample:

$$z_{\text{eff}} = \frac{\sum_{i=1}^{N_{\text{gal}}} w_{\text{tot},i} z_i}{\sum_{i=1}^{N_{\text{gal}}} w_{\text{tot},i}}, \quad (3)$$

where $w_{\text{tot},i}$ is the total weight of the i -th galaxy, given by $w_{\text{tot},i} = w_{c,i} w_{\text{FKP},i}$. For the random particles, the completeness weights are unity and hence the total weight for each random particle is equal to its FKP weight.

We generate the FKP weighted density field [50]:

$$F(\mathbf{x}) = n_g^w(\mathbf{x}) - \alpha_r n_r^w(\mathbf{x}), \quad (4)$$

by assigning the galaxies and random particles onto regularly-spaced grid points over a comoving cubic volume covering the whole survey region, where \mathbf{x} is the three-dimensional position of each FFT grid. The three-dimensional comoving coordinates of galaxies and random particles are computed from their angular positions and redshifts, assuming a reference cosmology (see below). In the equation above, $n_g^w(\mathbf{x})$ and $n_r^w(\mathbf{x})$ are the number density field of galaxies and of random particles, respectively, where the completeness weights are included for the galaxy field and the FKP weights are assigned to both the galaxies and random particles. α_r is a factor to adjust the local mean number density of randoms to that of galaxies, defined as $\alpha_r = N_{\text{gal}}^c / N_{\text{ran}}$, where N_{ran} is the total number of random particles.

For each of the two redshift bins and the two galactic hemispheres, we set a cube to perform FFTs so that their three side lengths are equal to one another and they contain all the galaxies and random particles. In addition, we keep zero-padding regions at least $200 h^{-1} \text{Mpc}$ in any direction. We determine the grid spacing for each FFT box according to the Nyquist wavenumber $k_{\text{Ny}} = 1.2 h \text{Mpc}^{-1}$. The evaluation of these density fields is done by summing up the total weights $w_{\text{tot},i}$ of galaxies or random particles assigned to each grid, divided by the volume of the grid cell. To assign the particles to grids, we use the piecewise cubic spline (PCS) [51] interpolation kernel. We also use the interlacing scheme [51] to mitigate the aliasing contamination, as well as the deconvolution of the PCS kernel in Fourier space.

Using these grid-based fields, we measure the power spectrum multipole of order ℓ with an estimator [48, 52–54]:

$$\hat{P}_\ell(k_i) = \frac{2\ell + 1}{A_{\text{norm}}} \frac{1}{N_i} \sum_{\mathbf{k} \in \text{bin } i} \tilde{F}_0(\mathbf{k}) \tilde{F}_\ell(-\mathbf{k}) - P_{\text{noise}} \delta_{\ell,0}^K, \quad (5)$$

where \mathbf{k} is a three-dimensional wavevector, the summation is taken over the wavevector modes which enter the i -th wavenumber bin, and N_i is the number of such modes. We split each wavevector into linearly spaced bins of wavenumber $k = |\mathbf{k}|$ with width $\Delta k = 0.01 h \text{Mpc}^{-1}$ in the range $k \in [0, 0.6] h \text{Mpc}^{-1}$. $\delta_{i,j}^K$ is the Kronecker delta that equals to unity if $i = j$ and zero otherwise. A_{norm} and P_{noise} are a normalization factor of the power spectrum and the shot noise, respectively, which we estimate from the galaxy and random catalogs as described below. In the equation above, we define

$$\tilde{F}_\ell(\mathbf{k}) \equiv \int d^3x F(\mathbf{x}) \mathcal{L}_\ell(\hat{\mathbf{k}} \cdot \hat{\mathbf{n}}) e^{-i\mathbf{k} \cdot \mathbf{x}}, \quad (6)$$

where $\hat{\mathbf{k}}$ is the unit vector of \mathbf{k} and $\hat{\mathbf{n}}$ denotes the angular direction along which the position \mathbf{x} is seen from an observer. Here we employ the local plane-parallel approximation [53, 54], *i.e.*, we adopt either one of two line-of-sight directions toward the points in the FKP field, to take into account the angular dependence of the redshift-space power spectrum. Following Ref. [48], we calculate

Name	Redshift	z_{eff}	N_{gal}	N_{gal}^c	α_r	$A_{\text{norm}} [h \text{ Mpc}^{-1}]$	$P_{\text{noise}} [h^{-3} \text{ Mpc}^3]$
low- z NGC	$0.2 < z < 0.5$	0.38	429182	445260.72	0.0206	8.092	3676.3
low- z SGC			174819	182676.6	0.0212	3.173	3363.3
high- z NGC	$0.5 < z < 0.75$	0.61	435741	467502.47	0.0205	8.977	7380.6
high- z SGC			158262	169907.44	0.0212	3.316	7856.7

TABLE I. Properties of the 4 galaxy samples, the low- z NGC, low- z SGC, high- z NGC and high- z SGC samples, in the CMASSLOWZTOT catalog we use in this work. Here NGC and SGC means the “North Galactic Cap” and “South Galactic Cap” fields in the SDSS survey footprints. We list the values of effective redshift (z_{eff}), unweighted and weighted numbers of galaxies (N_{gal} and N_{gal}^c), the ratio of the weighted galaxy number to random particle number (α_r), normalization (A_{norm}), and the shot noise term subtracted from the measured power spectrum monopole (P_{noise}), respectively. See the main text for details.

Eq. (6) as

$$\tilde{F}_\ell(\mathbf{k}) = \frac{4\pi}{2\ell+1} \sum_{m=-\ell}^{\ell} Y_{\ell m}^*(\hat{\mathbf{k}}) \left[\int d^3x F(\mathbf{x}) Y_{\ell m}(\hat{\mathbf{n}}) e^{-i\mathbf{k}\cdot\mathbf{x}} \right], \quad (7)$$

where $Y_{\ell m}$ is the spherical harmonics.

The normalization factor A_{norm} in Eq. (5) is defined as

$$A_{\text{norm}} \equiv \int d^3x [\bar{n}_g^w(\mathbf{x})]^2, \quad (8)$$

where $\bar{n}_g^w(\mathbf{x})$ is the mean galaxy number density at the position \mathbf{x} , including the completeness weights and the FKP weights. We estimate this factor by a summation over the random particles,

$$A_{\text{norm}} \approx \alpha_r \sum_{i=1}^{N_{\text{ran}}} \bar{n}_g(z_i) w_{\text{FKP},i}^2. \quad (9)$$

The shot noise we subtract from the measured monopole is calculated as

$$P_{\text{noise}} \equiv \frac{1 + \alpha_r}{A_{\text{norm}}} \int d^3x \bar{n}_g^w(\mathbf{x}) \quad (10)$$

$$\approx \frac{1}{A_{\text{norm}}} \left(\sum_{i=1}^{N_{\text{gal}}} w_{c,i}^2 + \alpha_r^2 \sum_{i=1}^{N_{\text{ran}}} \right) w_{\text{FKP},i}^2, \quad (11)$$

where the squares of both the completeness and FKP weights should be taken into account. In this paper, we ignore the shot noise contributions in the power spectrum multipoles of order $\ell \geq 2$. We list the values of A_{norm} and P_{noise} we estimate for each redshift bin and galactic hemisphere in Table I.

As the reference cosmology used to compute the comoving distances towards galaxies and randoms in the real survey data, we assume the flat-geometry Λ CDM model with $\Omega_m = 0.31$, which is the same as the model assumed in the measurement of the BOSS DR12 public spectra for their cosmology analysis [25].

Figure 1 shows the power spectrum multipoles that we measure from the catalogs. The symbols are the measured signals and error bars are the diagonal elements of

the power spectrum covariance matrix we estimate from the MULTIDARK-PATCHY (hereafter PATCHY) mock catalogs, as we describe in Sec. II B. We also show in the same figure the mean and variance of 2048 realizations of PATCHY mocks, by solid lines and shaded regions.

We found that our measurements are slightly different from those provided by the SDSS collaboration, which is also reported in Ref. [55]. We did a cross check of the measurement by using a publicly available Python code `nbodykit` (<https://nbodykit.readthedocs.io/en/latest/>) [56], and confirmed that the power spectra measured with this code and with our code agree well with each other, *e.g.*, typically within 0.3% for the monopole.

B. Covariance matrix from Patchy mock catalogs

To infer the cosmological parameters from the comparison between the theoretical predictions and measured power spectrum data, we need the covariance matrix. In this work, we estimate the power spectrum covariance using 2048 realizations of the PATCHY mock catalogs in Refs. [57, 58]. These mock catalogs were generated using an approximate N -body solver which combines the Lagrangian perturbation theory, a small-scale halo collapse model, and a semi-analytical galaxy biasing scheme, augmented by calibration to a reference large-volume N -body simulation sample selected from the BIGMULTIDARK simulations [59].

To measure the power spectrum multipoles from these mock catalogs, we employ the same estimator as applied to the observed galaxy data, including the interpolation kernel (PCS) and zero-padding size (at least $200 h^{-1} \text{ Mpc}$), but we set slightly a smaller Nyquist wavenumber $k_{\text{Ny}} = 1.0 h \text{ Mpc}^{-1}$ to reduce the computational time. In addition, we assume the cosmology with $\Omega_m = 0.307115$ which is used in the BIGMULTIDARK simulations to compute the comoving distance. We esti-

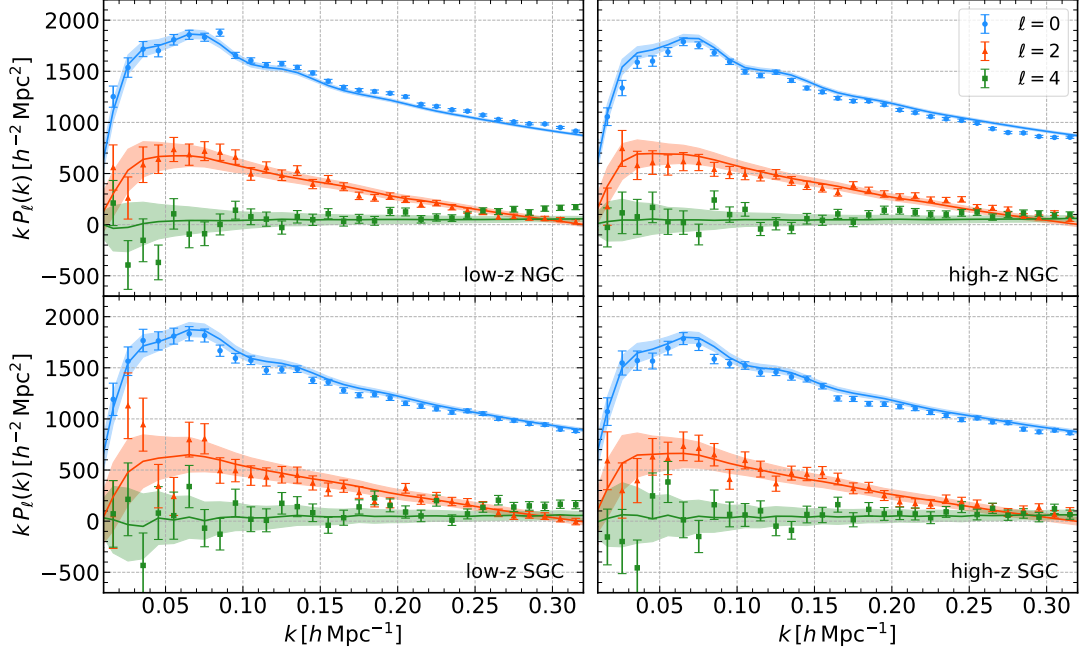


FIG. 1. Symbols with error bars are the monopole (blue), quadrupole (red), and hexadecapole (green) moments of the redshift-space power spectrum we measure from each of the four galaxy samples in Table I. The error bars are computed from the diagonal elements of the covariance matrix that is estimated from the 2048 realizations of the PATCHY mock catalogs. For comparison, the solid lines display the mean spectra in the PATCHY mock catalogs. The shaded region around the line denotes the range connecting the power spectrum errors in the k bins: the width of the shaded region is the same as the length of the error bar around the data point in each k bin.

mate the power spectrum covariance matrix as

$$\text{Cov} \left[\hat{P}_\ell(k_i), \hat{P}_{\ell'}(k_j) \right] = \frac{1}{N_r - 1} \sum_{n=1}^{N_r} \left[\hat{P}_\ell(k_i) - \bar{P}_\ell(k_i) \right] \left[\hat{P}_{\ell'}(k_j) - \bar{P}_{\ell'}(k_j) \right], \quad (12)$$

where $N_r = 2048$ is the number of PATCHY mock realizations, and we estimate the mean power spectrum as

$$\bar{P}_\ell(k_i) = \frac{1}{N_r} \sum_{n=1}^{N_r} \hat{P}_\ell(k_i). \quad (13)$$

We estimate the covariance matrix from the finite number of mock realizations and invert to obtain the estimate of the inverse covariance matrix. However, it leads to a biased estimation of the inverse covariance, even though the estimator of the covariance Eq. (12) is unbiased. To approximate the unbiased estimator of the inverse covariance, we multiply the so-called Hartlap factor [60] to the inverse of the estimated covariance:

$$f_{\text{Hartlap}} = \frac{N_r - n_{\text{bin}} - 2}{N_r - 1}, \quad (14)$$

where n_{bin} is the number of bins we use in the parameter inference. For instance, in the case that we

use the monopole, quadrupole and hexadecapole moments up to $k_{\text{max}} = 0.25 h \text{ Mpc}^{-1}$, the number of bins is $n_{\text{bin}} = 25 \times 3 = 75$ for each galaxy sample, yielding $f_{\text{Hartlap}} = 0.9629$.

III. THEORETICAL MODEL AND PARAMETERS

A. Theoretical model

To investigate the cosmological parameter constraint from the BOSS galaxy power spectrum, we use the theoretical template computed using the emulator for the redshift-space power spectrum of halos combined with the HOD model, developed in our previous work [36]. We below give a brief description of our theoretical template, and see Ref. [36] [also 17] for further details.

We employ the five-parameter HOD model in Ref. [43], which splits the galaxies into central and satellite galaxies. The mean halo occupation number of central and satellite galaxies within host halos with mass M are given as

$$\langle N_c \rangle(M) = \frac{1}{2} \left[1 + \text{erf} \left(\frac{\log M - \log M_{\text{min}}}{\sigma_{\log M}} \right) \right], \quad (15)$$

and

$$\begin{aligned}\langle N_s \rangle(M) &= \langle N_c \rangle(M) \lambda_s(M) \\ &\equiv \langle N_c \rangle(M) \left(\frac{M - \kappa M_{\min}}{M_1} \right)^{\alpha_{\text{sat}}},\end{aligned}\quad (16)$$

respectively, where $\text{erf}(x)$ is the error function and the logarithms in Eq. (15) are base 10. Note that, in our model we adopt $M \equiv M_{200} = (4\pi/3)200\bar{\rho}_{\text{m}0}R_{200}^3$ as the halo mass definition, where $\bar{\rho}_{\text{m}0}$ is the mean comoving mass density in the universe and R_{200} is the spherical comoving radius within which the mean mass density is 200 times $\bar{\rho}_{\text{m}0}$. Here $\{\log M_{\min}, \sigma_{\text{log } M}^2, \log M_1, \alpha_{\text{sat}}, \kappa\}$ are model parameters. The probability distribution of galaxies given the mean number is assumed to be Bernoulli for centrals and Poisson for satellites given that the halo of interest has a central halo. This HOD model is also used in the cosmology analysis of the galaxy-galaxy weak lensing and projected galaxy correlation function measured from the Hyper Suprime-Cam Year1 catalog and the BOSS DR11 catalog (Miyatake *et al.*, in prep.).

Using the above HOD model, our full model of the redshift-space galaxy power spectrum is given by the sum of the one- and two-halo terms,

$$P_{\text{gg}}(\mathbf{k}) = P_{\text{gg}}^{\text{1h}}(\mathbf{k}) + P_{\text{gg}}^{\text{2h}}(\mathbf{k}), \quad (17)$$

where

$$\begin{aligned}P_{\text{gg}}^{\text{1h}}(\mathbf{k}) &= \frac{1}{\bar{n}_{\text{g}}^2} \int dM \frac{dn}{dM}(M) \langle N_c \rangle(M) \\ &\times \left[2\lambda_s(M) \tilde{\mathcal{H}}(\mathbf{k}; M) + \lambda_s(M)^2 \tilde{\mathcal{H}}(\mathbf{k}; M)^2 \right],\end{aligned}\quad (18)$$

and

$$\begin{aligned}P_{\text{gg}}^{\text{2h}}(\mathbf{k}) &= \frac{1}{\bar{n}_{\text{g}}^2} \int dM_1 \frac{dn}{dM}(M_1) \left[\langle N_c \rangle(M_1) + \langle N_s \rangle(M_1) \tilde{\mathcal{H}}(\mathbf{k}; M_1) \right] \\ &\times \int dM_2 \frac{dn}{dM}(M_2) \left[\langle N_c \rangle(M_2) + \langle N_s \rangle(M_2) \tilde{\mathcal{H}}(\mathbf{k}; M_2) \right] \\ &\times P_{\text{hh}}(\mathbf{k}; M_1, M_2).\end{aligned}\quad (19)$$

These power spectra depend on the two-dimensional wavevector, $\mathbf{k} = (k_{\parallel}, k_{\perp})$ or $k(\mu, \sqrt{1 - \mu^2})$, due to the redshift-space distortion effect, where μ is the cosine angle between the wavevector \mathbf{k} and the line-of-sight direction $\hat{\mathbf{n}}$. In the above formulae, dn/dM is the halo mass function and \bar{n}_{g} is the global mean number density of galaxies defined as

$$\bar{n}_{\text{g}} = \int dM \frac{dn}{dM}(M) [\langle N_c \rangle(M) + \langle N_s \rangle(M)]. \quad (20)$$

For satellite galaxies, we model the intra-halo profile in redshift space as the multiplication of the Navarro-Frenk-White (NFW) profile [61] and the velocity distribution [17, 62, 63]:

$$\tilde{\mathcal{H}}(\mathbf{k}; M) = \tilde{u}_{\text{NFW}}(k; M) \tilde{\mathcal{F}}(k_{\parallel}; M), \quad (21)$$

where $\tilde{u}_{\text{NFW}}(k; M)$ is the Fourier transform of the NFW density profile normalized by halo mass M . To specify the NFW profile, we assume the median concentration-mass relation $c(M_{200})$ following the model in Refs. [64, 65]. $\tilde{\mathcal{F}}(k_{\parallel}; M)$ is the Fourier transform of the Gaussian velocity distribution whose velocity dispersion is given as

$$\mathcal{F}(\Delta r_{\parallel}; M) = \frac{1}{\sqrt{2\pi\sigma_v^2(M)}} \exp \left[-\frac{\Delta r_{\parallel}^2}{2\sigma_v^2(M)} \right]. \quad (22)$$

The velocity dispersion, $\sigma_v^2(M)$, is given by

$$\sigma_v^2(M) = \frac{1}{a^2 H^2} \frac{GM}{2aR_{200}(M)}, \quad (23)$$

where G is the gravitational constant, a is the scale factor, H is the Hubble parameter at scale factor a , and $R_{200}(M)$ is the halo radius R_{200} for halos with mass M . The factor $1/(aH)^2$ is to convert the velocity to the redshift-space displacement. The above velocity distribution models the fingers of God (FoG) effect due to virial motions of satellite galaxies in their host halos. In order to further include uncertainties in the FoG effect, we will introduce a nuisance parameter to model the uncertainty, $\sigma_v(M) \rightarrow c_{\text{vel}}\sigma_v(M)$, and treat c_{vel} as a model parameter in the cosmology analysis.

In this theoretical model, we use our emulator [36] to compute the redshift-space halo power spectrum $P_{\text{hh}}(\mathbf{k}; M_1, M_2)$ in the two-halo term (Eq. 19) for an input model in the flat Λ CDM cosmology. As described in Ref. [36], the emulator outputs $P_{\text{hh}}(\mathbf{k}; M_1, M_2)$ given as a function of the two-dimensional wavevector \mathbf{k} , rather than the multipole moments such as $P_{\text{hh},\ell}(k; M_1, M_2)$. This modeling allows us to straightforwardly include the AP effect, even in the presence of the FoG effect. We also use the publicly available **Dark Emulator** (<https://dark-emulator.readthedocs.io/en/latest/>) [38] to compute the halo mass function, and the **Colossus** code (<http://www.benediktdiemer.com/code/colossus/>) [66] to compute the halo concentration-mass relation. In the theoretical model the redshift-space halo power spectrum in the two-halo term, $P_{\text{hh}}(\mathbf{k}; M_1, M_2)$, carries cosmological information, and other functions such as the HOD and the distribution of galaxies in their host halos are all nuisance and are needed to account for uncertainties in the halo-galaxy connection.

B. Alcock-Paczyński effect

Since we need to assume a reference cosmology ($\Omega_{\text{m}} = 0.31$) in the measurement of the power spectrum, we incorporate the Alcock-Paczyński (AP) effect [67, 68] into the theoretical model. Due to the difference between the true and reference cosmologies, the Fourier-space

wavenumbers are transformed as

$$\begin{aligned} k_{\perp}^{\text{ref}} &= \alpha_{\perp} k_{\perp} \equiv \frac{D_A(z)}{D_A^{\text{ref}}(z)} k_{\perp}, \\ k_{\parallel}^{\text{ref}} &= \alpha_{\parallel} k_{\parallel} \equiv \frac{H^{\text{ref}}(z)}{H(z)} k_{\parallel}, \end{aligned} \quad (24)$$

where $D_A(z)$ and $H(z)$ are the angular diameter distance and Hubble parameter at the effective redshift z . Quantities with superscript “ref” denote those for the reference cosmology. By this coordinate transformation, the power spectrum multipole is transformed as

$$P_{\text{gg},\ell}^{\text{ref}}(k^{\text{ref}}) = \frac{2\ell+1}{2\alpha_{\perp}^2 \alpha_{\parallel}} \int_{-1}^1 d\mu^{\text{ref}} P_{\text{gg}}(k, \mu) \mathcal{L}_{\ell}(\mu^{\text{ref}}). \quad (25)$$

where k and μ in the argument of $P_{\text{gg},\ell}^{\text{ref}}$ are given in terms of k^{ref} and μ^{ref} ; $k = k(k^{\text{ref}}, \mu^{\text{ref}})$ and $\mu = \mu(\mu^{\text{ref}})$, given as

$$k(k^{\text{ref}}, \mu^{\text{ref}}) = k^{\text{ref}} \frac{1}{\alpha_{\perp}} \left[1 + (\mu^{\text{ref}})^2 \left(\frac{\alpha_{\perp}^2}{\alpha_{\parallel}^2} - 1 \right) \right]^{1/2}, \quad (26)$$

$$\mu(\mu^{\text{ref}}) = \mu^{\text{ref}} \frac{\alpha_{\perp}}{\alpha_{\parallel}} \left[1 + (\mu^{\text{ref}})^2 \left(\frac{\alpha_{\perp}^2}{\alpha_{\parallel}^2} - 1 \right) \right]^{-1/2}. \quad (27)$$

Since the reference cosmology is generally different from the underlying true cosmology, the AP effect induces an additional anisotropy in the measured power spectrum. In other words, the measured anisotropy enables us to infer the true cosmology through the geometrical information.

C. Survey window function

The FKP estimator we use to measure the power spectrum (see Sec. II A) estimates the power spectrum convolved with the survey window function. In this paper, we apply this convolution to the theoretical model rather than deconvolve the survey window from the measured power spectrum data. Following the procedure described in Ref. [24], we compute the window-convolved power spectrum multipoles as

$$P_{W,\ell}(k) = \int_0^\infty \frac{k'^2 dk'}{2\pi^2} \sum_L P_L(k') \left| \tilde{W}(k, k') \right|_{\ell L}^2, \quad (28)$$

where we denote the multipole moment of the survey window function in Fourier space as $\left| \tilde{W}(k, k') \right|_{\ell L}^2$, which we describe in Appendix A. $P_L(k)$ is the true power spectrum multipole and we use our model predictions of the power spectrum multipoles of order $L = 0, 2, 4$, and 6 in this summation. The multipole moments of the window function are confined to the regions where the difference between k and k' is small. Hence, to obtain

Parameter	Prior
Cosmological parameters	
ω_b	$\mathcal{N}(0.02268, 0.00038)$
ω_c	$\mathcal{U}(0.10782, 0.13178)$
Ω_Λ	$\mathcal{U}(0.54752, 0.82128)$
$\ln(10^{10} A_s)$	$\mathcal{U}(2.4752, 3.7128)$
n_s	$\mathcal{N}(0.9649, 0.0042)$
HOD parameters	
$\log M_{\text{min}}$	$\mathcal{U}(12.0, 15.0)$
$\sigma_{\log M}^2$	$\mathcal{U}(0.0001, 2.0)$
$\log M_1$	$\mathcal{U}(12.0, 16.0)$
α_{sat}	$\mathcal{U}(0.01, 5.0)$
κ	$\mathcal{U}(0.01, 5.0)$
Other nuisance parameters	
c_{vel}	$\mathcal{U}(0.01, 10.0)$
P_{shot}	$\mathcal{U}(-10^4, 10^4) h^{-3} \text{Mpc}^3$
Derived parameters	
Ω_m	—
H_0	—
σ_8	—

TABLE II. Model parameters and priors used in our cosmology analysis in flat Λ CDM cosmology. $\mathcal{N}(\mu, \sigma)$ denotes the Gaussian distribution with mean μ and standard deviation σ . $\mathcal{U}(a, b)$ denotes the uniform distribution between the minimum value a and the maximum value b . The Gaussian priors on ω_b and n_s are based on the BBN and *Planck* CMB constraints, respectively (see text for details). The flat priors on other cosmological parameters are set to be within the parameter ranges on which the emulator is supported.

the predictions up to $k_{\text{max}} \sim 0.3 h \text{Mpc}^{-1}$ used in this work, we safely truncate the integration in Eq. (28) up to $k = 0.6 h \text{Mpc}^{-1}$, the maximum wavenumber on which the emulator is supported.

D. Model parameters and priors

In this subsection, we describe the model parameters that we infer, as well as their prior settings. The default setting is summarized in Table II.

1. Cosmological parameters

Since we want to infer the cosmological parameters within the flat-geometry Λ CDM framework, we sample all of the five parameters:

$$\mathbf{p}_{\text{cosmo}} = \{\omega_b, \omega_c, \Omega_\Lambda, \ln(10^{10} A_s), n_s\}, \quad (29)$$

where $\omega_b = \Omega_b h^2$ and $\omega_c = \Omega_c h^2$ are the physical energy density parameters of baryon and cold dark matter,

Ω_Λ is the energy density parameter of the cosmological constant, and A_s and n_s are the amplitude (at the pivot scale $k_{\text{pivot}} = 0.05 \text{ Mpc}^{-1}$) and the spectral tilt of the power spectrum of primordial curvature perturbations. For ω_b and n_s , we impose priors that are inferred from other cosmological probes. More specifically, we adopt a Gaussian prior on ω_b from the primordial deuterium and helium abundance data compared with the standard Big Bang nucleosynthesis (BBN) model [46, 69, 70]. On the other hand, we impose a Gaussian prior on n_s given in Table 1 of Ref. [47] for the *Planck* 2018 TT,TE,EE+lowE+lensing. We treat $\Omega_m (= 1 - \Omega_\Lambda)$, the total matter energy density, $H_0 = 100h \text{ km s}^{-1} \text{ Mpc}^{-1}$, the Hubble constant, and σ_8 , the standard deviation of linear matter perturbations at $z = 0$ averaged within a sphere with comoving radius $8h^{-1} \text{ Mpc}$, as the derived parameters. We fix the density parameter of neutrinos to $\omega_\nu = 0.00064$, corresponding to 0.06 eV for the total mass of the three mass eigenstates, which is used when computing the linear matter power spectrum used to set up the initial conditions of cosmological simulations that are used for the DARK EMULATOR development [38].

2. Nuisance parameters

As we described in Sec. III A, we employ five parameters to specify the HOD model for each galaxy sample. In addition, we include two additional nuisance parameters.

- c_{vel} — The multiplicative coefficient on the velocity dispersion of galaxies relative to the halo center. It regulates the uncertainty on the strength of the FoG effect (see around Eq. 22).
- P_{shot} — The residual shot noise contribution apart from the simple Poisson shot noise. We add P_{shot} to the galaxy power spectrum $P_{\text{gg}}(k, \mu)$, and hence it is relevant only to the monopole moment.

We employ a flat prior over the range $[-10^4, 10^4] (h^{-1} \text{ Mpc})^3$ for the latter. The mean number density of galaxies for each sample is a factor of a few times $10^{-4} (h^{-1} \text{ Mpc})^3$ (Table I), so the prior range is sufficiently wide. Thus, we have seven nuisance parameters on the halo-galaxy connection:

$$\mathbf{p}_{\text{galaxy}} = \{\log M_{\text{min}}, \sigma_{\log M}^2, \log M_1, \alpha_{\text{sat}}, \kappa, c_{\text{vel}}, P_{\text{shot}}\}, \quad (30)$$

for each of the 4 galaxy samples in Table I. Hence, the total number of parameters is $5 + 7 \times 4 = 33$ within the flat Λ CDM framework.

As can be found from Table II, we employ a broad prior range for each of the halo-galaxy connection parameters. For example, the range of M_{min} , which is one of the parameters that are sensitive to the linear bias of the galaxy sample, corresponds to halos that have $b_1 \simeq [1.2, 10.2]$ at $z = 0.5$ for the *Planck* cosmology. Thus our approach can be considered conservative in parameter inference.

E. Parameter inference

We employ the Bayesian inference to derive the parameter posterior distribution:

$$p_{\text{post}}(\mathbf{p}|\mathcal{D}) \propto \mathcal{L}(\mathcal{D}|\mathbf{p})p_{\text{prior}}(\mathbf{p}), \quad (31)$$

where p_{prior} and p_{post} are the prior and posterior distributions of model parameters, and $\mathcal{L}(\mathcal{D}|\mathbf{p})$ is the likelihood function of the observational data \mathcal{D} given parameters \mathbf{p} . Using the power spectrum data vector and the covariance matrix, we compute the log-likelihood function:

$$\ln \mathcal{L}(\mathcal{D}|\mathbf{p}) = -\frac{1}{2} \sum_{\text{samp}} \sum_{\ell, \ell'} \sum_{i,j}^{k_{\text{max}}} [P_\ell^{\mathcal{D}}(k_i) - P_\ell(k_i; \mathbf{p})] \times \text{Cov}^{-1}[P_\ell(k_i), P_{\ell'}(k_j)] [P_{\ell'}^{\mathcal{D}}(k_j) - P_{\ell'}(k_j; \mathbf{p})], \quad (32)$$

where we assume the Gaussian likelihood and omit the normalization factor. $P_\ell^{\mathcal{D}}(k_i)$ denotes the data of the ℓ -th multipole moment of the power spectrum in the i -th wavenumber bin, $P_\ell(k_i; \mathbf{p})$ is its theoretical model prediction, and \mathbf{p} is the model parameters. We include the power spectrum information over $k_{\text{min}} \leq k \leq k_{\text{max}}$, and we employ $k_{\text{min}} = 0.005 h \text{ Mpc}^{-1}$ and $k_{\text{max}} = 0.25 h \text{ Mpc}^{-1}$ as our fiducial choices, respectively. We will below give a validation of the choice of $k_{\text{max}} = 0.25 h \text{ Mpc}^{-1}$ and discuss how different choices of k_{min} or k_{max} change the cosmological results. The summation \sum_{samp} denotes the summation over galaxy samples when the power spectrum information for different galaxy samples are combined.

For the parameter sampling, we employ the Markov-chain Monte Carlo (MCMC) sampling of the standard Metropolis algorithm [71], or the nested sampling algorithm MultiNest [72] implemented in the public Python package PyMultiNest. In the MCMC sampling, we monitor the convergence for the cosmological parameters by using a method in Ref. [73], which is an improved variant of the Gelman-Rubin diagnostic [74, 75]. More specifically, we apply the rank-normalization [73] to the MCMC chains and measure the Gelman-Rubin statistic \hat{R} of the chains split in half (so-called the split- \hat{R} [76]), after discarding 1000 points at the beginning of each chain as the burn-in phase. We run the MCMCs until the criteria $\hat{R} < 1.05$ for the cosmological parameters are met.

We should note that, throughout this paper, we *do not* include the abundance of galaxies (the mean number density) nor the BAO information after reconstruction [*e.g.*, see 77, for such a study] in the data vector in the parameter inference.

IV. RESULTS

We show the main results of our cosmology analysis in this section. Throughout this paper, we mainly focus on the constraints on three cosmological parameters Ω_m , H_0 , and σ_8 , which are well constrained by the redshift-space galaxy power spectrum, in flat Λ CDM model.

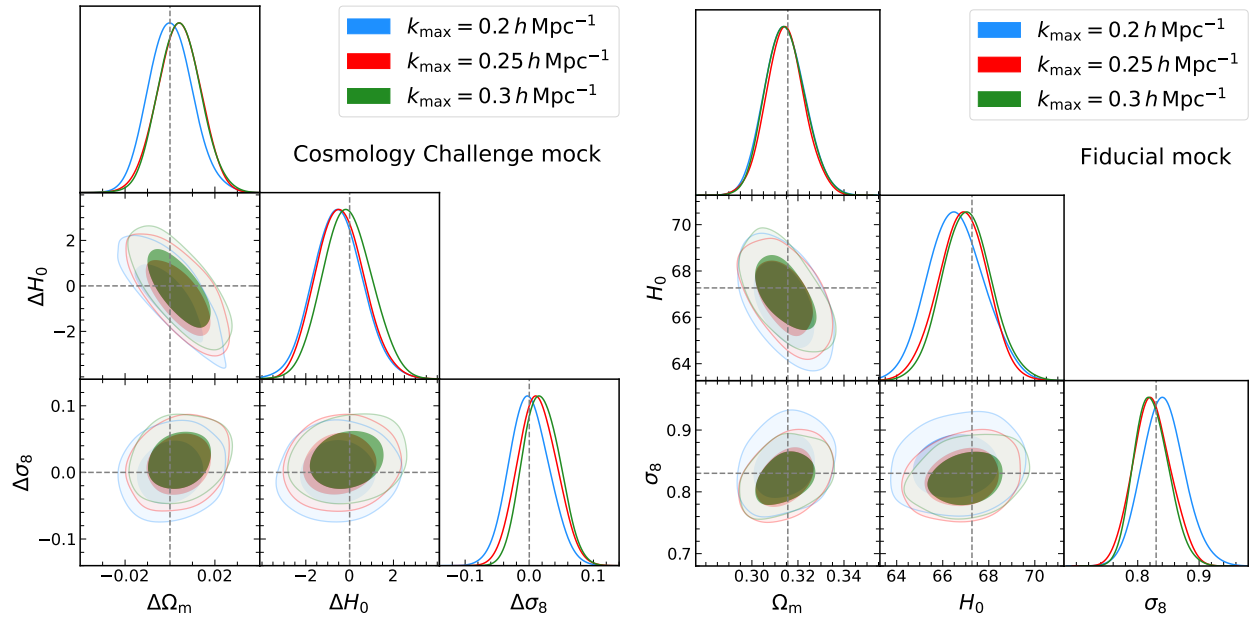


FIG. 2. Results of validation tests of our cosmology analysis pipeline: we apply the analysis pipeline to the mock signals for the 4 BOSS-like galaxy samples (see Table I) using the covariance matrix of the actual BOSS spectra. We include the monopole, quadrupole and hexadecapole moments of the redshift-space power spectrum for each of the 4 galaxy samples over $0.005 h \text{ Mpc}^{-1} \leq k \leq k_{\text{max}}$, and we show the results for $k_{\text{max}} = 0.20, 0.25$ or $0.30 h \text{ Mpc}^{-1}$, respectively. The contours show the posterior distributions of Ω_m, H_0 , and σ_8 including marginalization over uncertainties in other parameters including the halo-galaxy connection parameters. The left plot shows the results for the galaxy mocks that are generated using a different recipe of the halo-galaxy connection from our fiducial HOD model: the mock galaxy catalogs used in the Cosmology Challenges in Ref. [35] (see text for details). Since we would like to blind the true values of the cosmological parameters, we show the results in terms of the parameter difference such as $\Delta\Omega_m = \Omega_m - \Omega_{m,\text{true}}$. The right plot shows the results for the mock catalogs generated using the same form of HOD model as in our HOD model. The dashed lines in the right panel are the true values of the cosmological parameters used in the mock catalogs, *i.e.*, those for the *Planck* cosmology.

A. Validation tests

Before showing the main results, we first present validation tests of our emulator based method. To test the validity and usefulness of the emulator-based method, we performed various cosmology challenges: we apply our cosmology analysis pipeline to simulated mock signals of the redshift-space galaxy power spectrum to address whether the pipeline can recover the underlying true cosmological parameters used in the simulations. Please see Ref. [35] for details of the procedures and aims. Y. K., who is one of the authors of this paper and led the actual cosmology inference analysis of the BOSS data, applied the pipeline to the mock signals for the BOSS-like galaxies used in [35]. The mock galaxy catalogs were generated using a different recipe for the halo-galaxy connection based on subhalos, so it is not entirely clear whether our HOD method can recover the underlying cosmological parameters. For instance, the spatial and velocity structures of satellite galaxies in host halos are generally different from those in our fiducial halo model. In this test, Y. K. was not informed of the cosmological parameters, and the validation test was done effectively in a blind manner.

He submitted the results to T. N., who is a co-author of this paper and is the main organizer and the maintainer of the challenge program, and then the ground truth cosmological parameters were revealed with the mutual agreement not to update the analysis anymore. The submitted results are recorded and presented on the challenge webpage (<https://www2.yukawa.kyoto-u.ac.jp/~takahiro.nishimichi/data/PTchallenge/>).

In Figure 2 we show the results of our validation tests. The left panel shows the results using the simulated signals that are generated from the mock catalogs of the above cosmology challenges of Ref. [35]. To mimic the cosmology analysis of the BOSS power spectra, we use the mock catalogs at $z = 0.38$ and 0.61 to simulate the redshift-space spectra for the 4 subsamples, the NGC/SGC in the low- z and high- z bins (Table I), and use the same covariance matrix as that used in the following cosmology analysis of BOSS spectra (see Sec. IIB). To generate the mock catalogs we used the realizations of N -body simulations for the total volume of $566 (h^{-1} \text{ Gpc})^3$, which is about a hundred times that of the BOSS DR12 galaxy sample. The large volume of the simulations allows us to sufficiently reduce the sample variance errors in the simulated power spectra. Therefore, we can conduct a fairly stringent test of the sys-

tematic error due to an imperfect modeling of the power spectrum. The figure shows that our analysis method recovers the true cosmological parameters to within the statistical errors of the BOSS galaxy spectra. We also stress that our emulator-based method passes the validation test even if including the power spectrum information up to $k_{\text{max}} = 0.3 h \text{ Mpc}^{-1}$, where the perturbation theory breaks down. Here the constraints on Ω_m and H_0 are mainly from the BAO features and partly from the power spectrum shape via the AP effect. On the other hand, the constraint on σ_8 is from the power spectrum amplitude, after the degeneracies with galaxy bias uncertainty (uncertainties in the halo-galaxy connection in our model) are lifted by measurements of the RSD effect as we will discuss later (Sec. VF). However, including the information beyond $k \simeq 0.2 h \text{ Mpc}^{-1}$ gives little improvement in the cosmological parameters, due to the shot noise domination and the degeneracies with the halo-galaxy connection parameters. On the other hand, we find that the constraints on HOD parameters are improved by including the higher- k information.

As another sanity check, we also perform the validation tests using the mock galaxy catalogs in Refs. [17, 38], which are generated from the simulations for the *Planck* cosmology using the same HOD prescription as that in our analysis. Similarly to the above test, we used the outputs of N -body simulations at $z = 0.251$ and 0.617 , adopted the same HOD model as that in Ref. [78] to populate galaxies into halos of each realization, and then simulated the mock galaxy spectra for the 4 galaxy samples. We used the simulations of total volume $128 (h^{-1} \text{ Gpc})^3$ to generate the simulated data vector [see 17, for details of the simulations], and performed the cosmology analysis using the same covariance matrix of the BOSS spectra. The right panel of Figure 2 shows that our analysis method recovers the cosmological parameters to within the statistical errors, for all the k_{max} values. One might notice a slight bias in each cosmological parameter, even if both the theoretical template and the mock catalogs employ the same form of HOD model. We ascribe the parameter shift to the projection effect of the full posterior distribution in a multi-dimensional parameter space [see 79, for the similar discussion]. Here we note that some of the halo-galaxy connection parameters are not necessarily recovered by the analysis as explicitly shown in Figure 13 of Appendix B. The figure in the appendix also shows that including the power spectrum information on the higher k_{max} gives smaller error bars for the halo-galaxy connection parameters, although the central values are biased for some of the halo-galaxy parameters. On the other hand, the credible intervals of the cosmological parameters are not much improved as can be found from Figure 2. Hence, from these results, we conclude that our method can robustly recover the cosmological parameters to within the statistical errors of the BOSS power spectra, after marginalization over the halo-galaxy connection parameters. Here note that the cosmological information is extracted from the

redshift-space power spectrum of halos predicted by the emulator in our method. In this paper, we employed $k_{\text{max}} = 0.25 h \text{ Mpc}^{-1}$ as our fiducial choice of the maximum wavenumber.

We will also later show the validation test of our analysis method using the mock catalogs including the assembly bias effect, which is one of the most dangerous, physical systematic effects in the halo model approach.

B. Results: Λ CDM cosmology

Figure 3 shows the main results of this paper: the projected posterior distributions of Ω_m , H_0 and σ_8 for the flat Λ CDM model, after marginalizing over the other parameters such as the halo-galaxy connection parameters. These constraints include the BAO and full shape information of the redshift-space power spectrum for the 4 samples of the low- z /high- z NGC and SGC samples, up to $k_{\text{max}} = 0.25 h \text{ Mpc}^{-1}$ where the nonlinear effects such as nonlinear bias, nonlinear clustering and nonlinear RSD are properly included. Our method achieves precise measurements of the cosmological parameters:

$$\begin{aligned}\Omega_m &= 0.3000^{+0.0113}_{-0.0108} \\ H_0 &= 68.35^{+1.21}_{-1.39} \\ \sigma_8 &= 0.7417^{+0.0345}_{-0.0364},\end{aligned}\tag{33}$$

where we report the mode and the 68% credible interval of the marginalized posterior distribution for each parameter, respectively. Note that H_0 is in units of $\text{km s}^{-1} \text{ Mpc}^{-1}$. It is interesting to note that our results are consistent with those in Ref. [26] to within the statistical errors, which uses the EFTofLSS as the theoretical template to compare with the redshift-space power spectrum for the same BOSS samples, even though our halo model-based method and the EFTofLSS are constructed based on totally different frameworks. The size of the error bar in each parameter is comparable with that of the EFTofLSS result. This might be counter-intuitive, because one might think that our halo model based method is a more restrictive model than the EFTofLSS model, so expect our method gives tighter constraints on the cosmological parameters. Probably this is due to the wide priors of the halo-galaxy connection parameters in our analysis, and we will later discuss a possible room of improvements in the cosmological parameters within our method.

Our results can also be compared with the *Planck* 2018 CMB constraints: we overplot the *Planck* 2018 cosmological constraints from the baseline likelihood of “TT, TE, EE+lowE”; the MCMC chains of *Planck* 2018 cosmology analysis are downloaded from the Planck Legacy Archive (<http://pla.esac.esa.int/pla/#cosmology>), where the neutrino mass is fixed to 0.06 eV as we did in our analysis. Our results are in good agreement with the *Planck* results for H_0 and Ω_m , but display a slight tension for σ_8 . This might be in a similar line with the

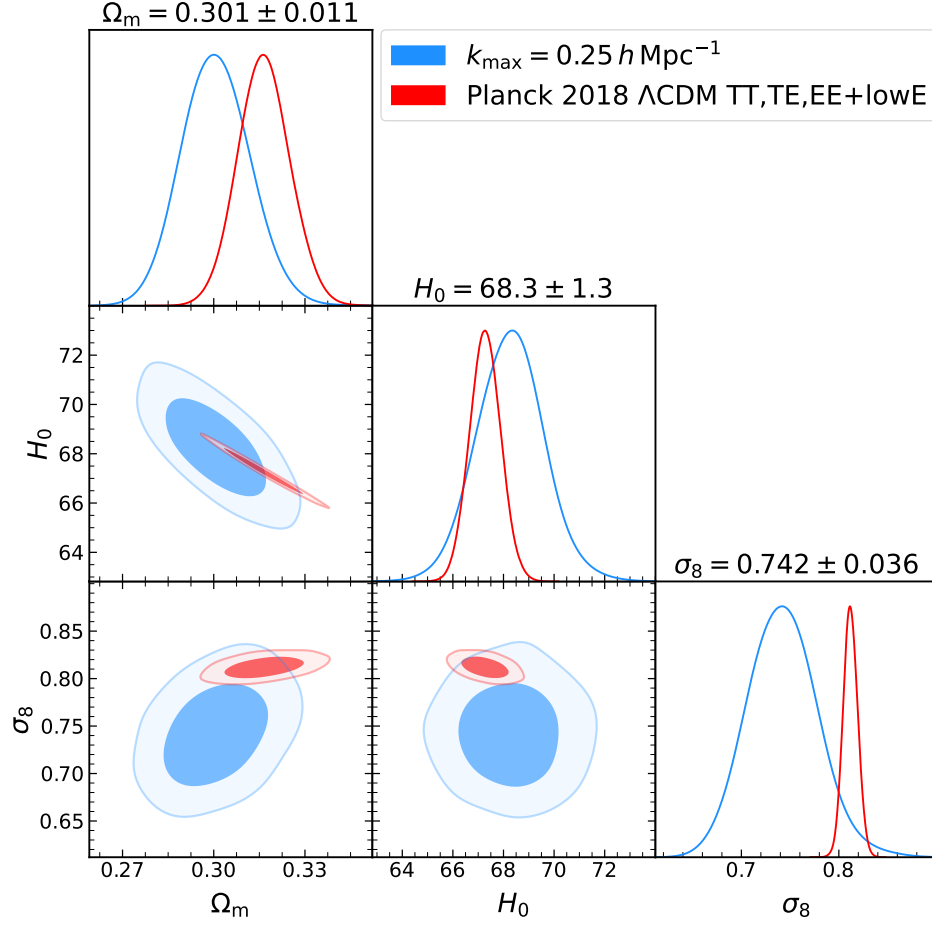


FIG. 3. The posterior distributions of Ω_m , H_0 and σ_8 , obtained from the cosmology inference including the full shape of the monopole, quadrupole and hexadecapole moments of the redshift-space power spectra up to $k_{\text{max}} = 0.25 h \text{ Mpc}^{-1}$ for the BOSS DR12 galaxy catalogs, for the flat ΛCDM model. For the theoretical templates we use the emulator-based halo model, and the posteriors include marginalization over uncertainties in other cosmological parameters and the nuisance parameters including the halo-galaxy connection parameters. For comparison, the red contours show the results from the *Planck* 2018 “TT,TE,EE+lowE” analysis.

Parameter	MAP	Median	68% CI	Planck 68% CI
$\ln(10^{10} A_s)$	2.878	2.900	$2.904^{+0.086}_{-0.096}$	3.045 ± 0.016
Ω_m	0.3085	0.3003	$0.3000^{+0.0113}_{-0.0108}$	0.3166 ± 0.0084
$H_0 [\text{km s}^{-1} \text{ Mpc}^{-1}]$	67.65	68.25	$68.35^{+1.21}_{-1.39}$	67.27 ± 0.60
σ_8	0.7384	0.7413	$0.7417^{+0.0345}_{-0.0364}$	0.8120 ± 0.0073
$S_8 \equiv \sigma_8(\Omega_m/0.3)^{0.5}$	0.7488	0.7417	$0.7402^{+0.0429}_{-0.0414}$	0.834 ± 0.016
$f\sigma_8(z_{\text{eff}} = 0.38)$	0.4359	0.4466	$0.4460^{+0.0316}_{-0.0313}$	0.4771 ± 0.0066
$f\sigma_8(z_{\text{eff}} = 0.61)$	0.4220	0.4172	$0.4141^{+0.0293}_{-0.0265}$	0.4696 ± 0.0053

TABLE III. The results of the cosmological parameter inference of the BOSS power spectra for ΛCDM model as in Figure 3. Note that we include the BBN prior on ω_b and the *Planck* prior on the spectral tilt n_s (see Table II). For each parameter, we show the parameter value at the *maximum a posteriori* (MAP), the median, and the mode with 68% credible interval (CI) for the 1d posterior distribution of each parameter. The parameters other than $\ln(10^{10} A_s)$ are derived parameters (see Table II). For comparison with constraints from other experiments, we also show the constraints on $S_8 \equiv \sigma_8(\Omega_m/0.3)^{0.5}$ and $f(z)\sigma_8(z)$, where f is the linear growth rate $f \equiv d \ln D / d \ln a$. For $f\sigma_8$, we show the results obtained from the cosmology analysis using the subsample of low- z NGC+SGC or high- z NGC+SGC sample at the effective redshift $z_{\text{eff}} = 0.38$ and 0.61 , respectively (see the right panel of Figure 6). For comparison, we also show the 68% credible interval from the *Planck* 2018 “TT,TE,EE+lowE” analysis, taken from Table 2 of Ref. [47].

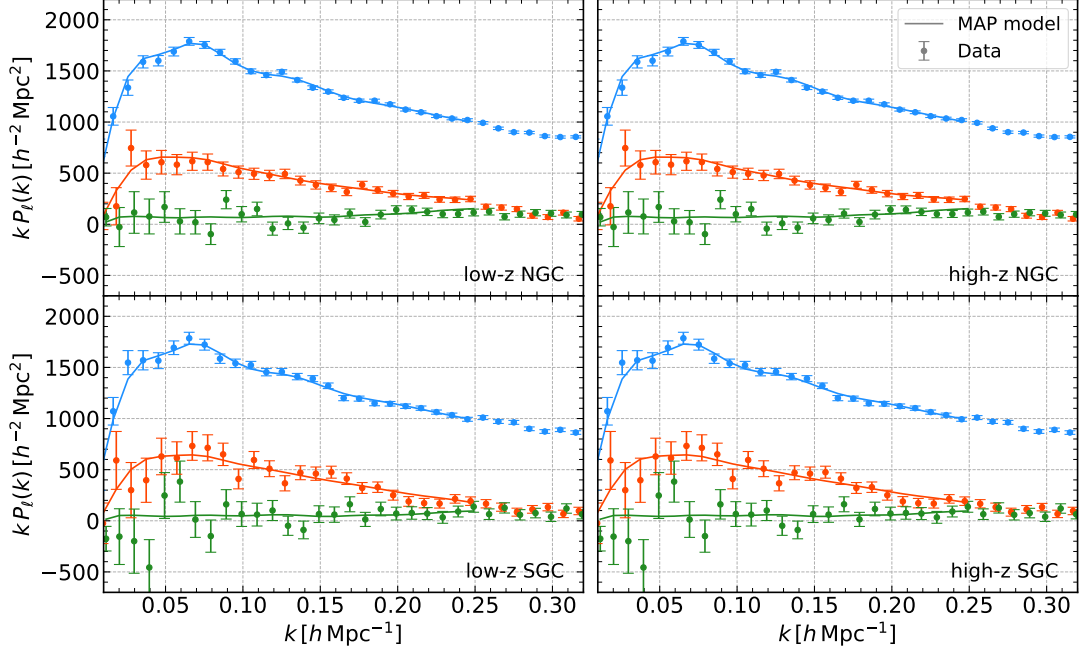


FIG. 4. The comparison of monopole (blue), quadrupole (red), and hexadecapole (green) moments between the measurements and the model predictions at MAP of the MCMC chains in our cosmological analysis shown in Figure 3. The data points and the error bars are the same as those in Figure 1.

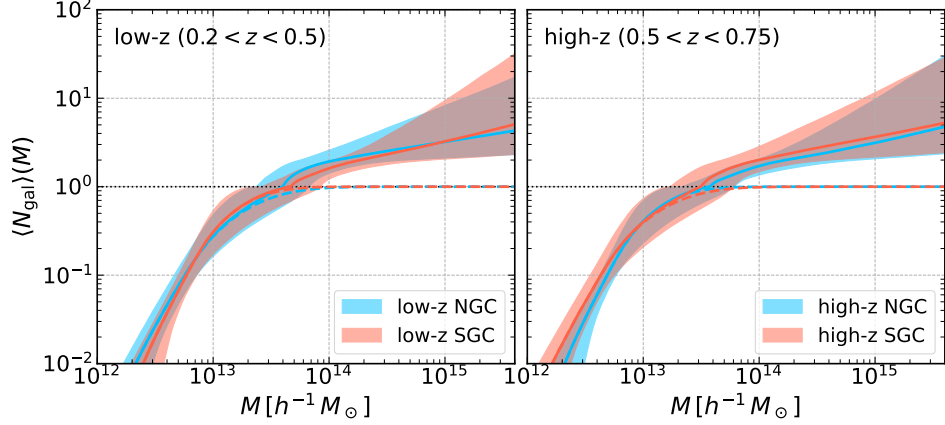


FIG. 5. The median and 68% percentile interval of the HOD functions for each of the BOSS galaxy samples (low- z /high- z NGC/SGC samples), obtained from the MCMC chains in Figure 3. The solid and dashed lines are the medians of central+satellite and central-only HOD functions, respectively.

so-called σ_8 tension reported from the weak lensing surveys [80–83]. However, the significance is not sufficient, so further investigation is needed. In Table III, we also show the parameter value at the *maximum a posteriori* (MAP), the median, and the mode with 68% credible interval (CI) for the 1d posterior distribution of each parameter. For comparison with the weak lensing survey results [*e.g.* 80], we also give the results for S_8 , the parameter on which the weak lensing surveys can give most stringent constraint. In addition, we show the results for $f(z)\sigma_8(z)$, which is the parameter often used to characterize the constraint mainly from the RSD measurement. The table gives the constraints for $f(z)\sigma_8(z)$ that are obtained from the MCMC analyses using either of the low- z NGC+SGC sample or high- z NGC+SGC sample at the effective redshift $z_{\text{eff}} = 0.38$ or 0.61 , respectively (see below). Note that our constraint is from the combined information of the BAO, the AP effect, the RSD effect and the amplitude and shape information of the power spectrum under the flat Λ CDM framework. Our results are consistent with those of Ref. [26], but are slightly lower than those in Ref. [5].

Figure 4 shows that our model at MAP well reproduces all the measured multipoles of redshift-space power spectra. Compared with Figure 1, our model appears to give a slightly better agreement with the BOSS spectra for the galaxy samples than the PATCHY mock catalogs do. The reduced chi-square value at the MAP is $\chi^2/\text{d.o.f.} \simeq 1.08$ for $267 (= 300 - 33)$ degrees of freedom (the p -value $p \simeq 0.18$), implying that the MAP model gives a reasonable fit to the data. Taking a closer look at the figure, our model has a slightly weaker BAO feature than data. This tendency reflects the fact that our power spectrum emulator is based on the training datasets which have a larger k -bin width ($\Delta k = 0.02 h \text{ Mpc}^{-1}$) than the data ($\Delta k = 0.01 h \text{ Mpc}^{-1}$), to suppress the statistical scatters on the training data (also see Appendix A of Ref. [36]). Since the BAO feature leads to a tight constraint on Ω_m through the AP effect, the sharpening of the BAO feature in the emulator could improve the cosmological constraints.

Figure 5 shows the mean HOD functions obtained from the MCMC chains. It can be found that the galaxy population inferred from the BOSS DR12 galaxy power spectra is almost confined to halos with masses, $M \gtrsim 10^{12} h^{-1} M_\odot$. This figure also shows that there is no remarkable difference in the HOD among the 4 galaxy samples. Our results are qualitatively consistent with the HODs estimated in the previous works [84–86]. We again stress that the HOD constraints are obtained from the fitting of the emulator-based halo model to the redshift-space power spectrum, without employing any strong priors on the HOD parameters nor using the abundance information (the mean number density of galaxies). Hence, the posterior distributions of HOD are purely from the redshift-space clustering information, while the previous works took into account different clustering information such as the galaxy-galaxy weak lensing and/or the pro-

jected correlation function.

V. DISCUSSION

In this section, we discuss the robustness of our cosmology results: we study how different analysis methods and datasets change the inferred cosmological parameters.

A. Variations in the cosmological parameters for different galaxy subsamples

In Figure 6 we study how the cosmological parameters are changed when using different subsets of the data vector: the left panel shows the results for 4 individual galaxy samples, and the right panel shows the combined results for each of the two redshift bins, where the two galactic hemispheres, NGC and SGC, are combined. Shifts in each parameter display a similar trend to those shown in Figure 2 of Ref. [26], even though we use a totally different theoretical template, *i.e.*, the halo model based method, compared to the EFTofLSS in their paper. Hence, we think that the parameter shifts are likely due to the sample variances in each subsample. For completeness of our discussion, in Appendix C we show the 2d posterior distributions for the full parameters for each of the 4 individual galaxy samples (see Figure 14). The low- z SGC sample displays a sizable difference in some parameters compared to the other samples, but the difference is still within the statistical errors. Hence, we cannot give any definite conclusion as to that sample could have a potential observational systematics compared to the others.

B. The impact of hexadecapole moments

Figure 7 shows that the inclusion of the hexadecapole moment of the redshift-space power spectrum for each sample yields only a subtle improvement in the cosmological parameters, because the hexadecapole moments have lower signal-to-noise ratios than the monopole and quadrupole moments as shown in Figure 4. However, we note that the hexadecapole indeed improves some of the HOD parameters, which is consistent with the finding in Ref. [87].

C. The cosmological information in the different range of k

One advantage of our approach, *e.g.*, compared to the perturbation theory based method such as the EFTofLSS, is that ours enables to compare the model predictions with the measurements up to higher k_{max} . As described in our previous paper [36], our emulator is

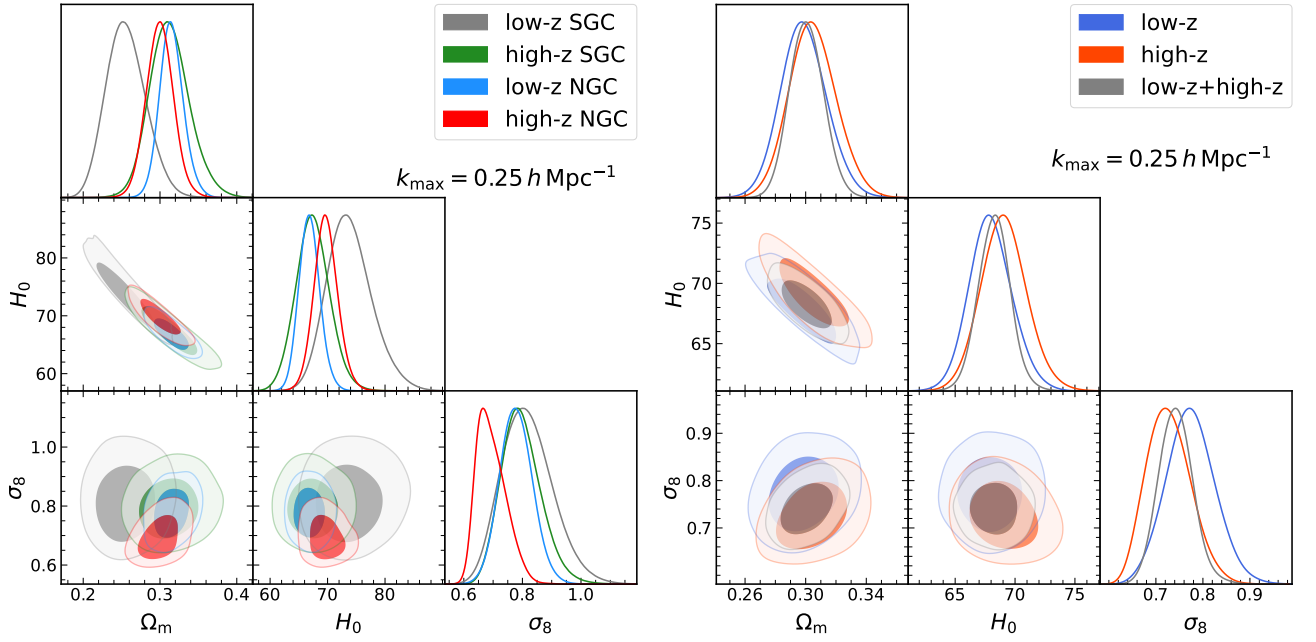


FIG. 6. The posterior distributions for cosmological parameters, obtained from the different galaxy subsamples. The left panel shows the results for 4 individual galaxy samples: low- z NGC, low- z SGC, high- z NGC, and high- z SGC (see Table I). The right panel shows the results for each of low- z or high- z NGC+SGC samples. In the right panel, we overplot the gray contours to show the distribution for the full sample for comparison, which is the same as the blue contours in Figure 3. These results can be compared with Figure 2 in Ref. [26], which shows the similar posterior distributions obtained using the EFTofLSS.

Parameter	low- z NGC			low- z SGC		
	MAP	Median	68% CI	MAP	Median	68% CI
$\ln(10^{10} A_s)$	3.004	2.997	$3.000^{+0.139}_{-0.136}$	3.157	3.070	$3.075^{+0.194}_{-0.206}$
Ω_m	0.3104	0.3144	$0.3136^{+0.0153}_{-0.0145}$	0.2386	0.2545	$0.2517^{+0.0275}_{-0.0232}$
H_0 [km s $^{-1}$ Mpc $^{-1}$]	66.69	66.77	66.77 ± 1.75	74.32	73.61	$73.14^{+4.01}_{-3.54}$
σ_8	0.7752	0.7771	$0.7764^{+0.0548}_{-0.0540}$	0.8154	0.8112	$0.8030^{+0.0884}_{-0.0818}$
$S_8 \equiv \sigma_8(\Omega_m/0.3)^{0.5}$	0.7886	0.7956	$0.7892^{+0.0681}_{-0.0570}$	0.7271	0.7460	$0.7282^{+0.0985}_{-0.0775}$
$f\sigma_8(z_{\text{eff}} = 0.38)$	0.4532	0.4558	$0.4531^{+0.0362}_{-0.0314}$	0.4409	0.4471	$0.4388^{+0.0540}_{-0.0447}$
Parameter	high- z NGC			high- z SGC		
	MAP	Median	68% CI	MAP	Median	68% CI
$\ln(10^{10} A_s)$	2.480	2.682	$2.611^{+0.184}_{-0.084}$	3.001	3.028	$3.034^{+0.163}_{-0.176}$
Ω_m	0.3054	0.2995	$0.3000^{+0.0168}_{-0.0177}$	0.3038	0.3113	$0.3088^{+0.0268}_{-0.0234}$
H_0 [km s $^{-1}$ Mpc $^{-1}$]	69.67	69.65	$69.50^{+2.14}_{-1.86}$	66.99	67.35	$67.23^{+2.95}_{-2.74}$
σ_8	0.6284	0.6876	$0.6652^{+0.0651}_{-0.0304}$	0.7616	0.7912	$0.7838^{+0.0695}_{-0.0613}$
$S_8 \equiv \sigma_8(\Omega_m/0.3)^{0.5}$	0.6340	0.6860	$0.6664^{+0.0721}_{-0.0431}$	0.7664	0.8054	$0.7938^{+0.0827}_{-0.0710}$
$f\sigma_8(z_{\text{eff}} = 0.61)$	0.3616	0.3942	$0.3816^{+0.0383}_{-0.0194}$	0.4380	0.4565	$0.4493^{+0.0436}_{-0.0334}$

TABLE IV. Similar to Table III, but this table shows the results obtained from the cosmology analysis using each of the 4 galaxy samples in Table I.

designed to give an accurate prediction of the redshift-space power spectrum up to $k = 0.6 h \text{ Mpc}^{-1}$. However the power spectrum measurements at $k \gtrsim 0.2 h \text{ Mpc}^{-1}$ are in the shot noise dominated regime, and therefore it is not clear whether the cosmological parameters are improved even if we include the data points at higher wavenumbers. In Figure 8 we study how the cosmologi-

cal parameters are changed for different choices of k_{max} ; we consider $k_{\text{max}} = 0.2, 0.25$ or $0.3 h \text{ Mpc}^{-1}$, respectively. The figure shows that the size of the credible intervals is not largely changed for the different k_{max} values, confirming the shot noise domination in the power spectrum measurements at $k \gtrsim 0.2 h \text{ Mpc}^{-1}$. We confirmed that the statistical errors of the halo-connection parameters

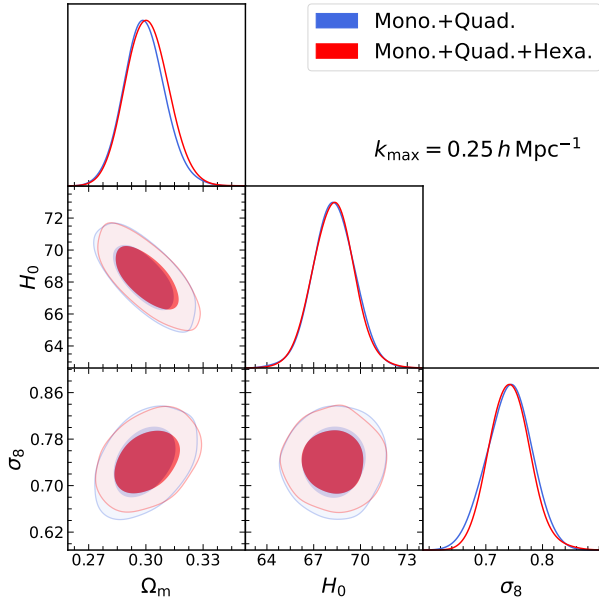


FIG. 7. The posterior distributions of cosmological parameters in our fiducial cosmology analysis for the full galaxy sample, obtained if or not we include the hexadecapole moments of the redshift-space power spectrum for each sample in the parameter inference. The red contours are the same as those in Figure 3.

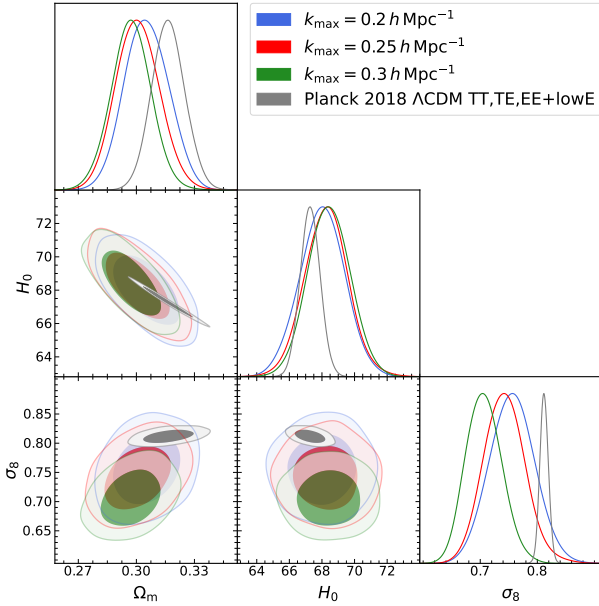


FIG. 8. Comparison of the posterior distributions obtained when including the redshift-space power spectrum information up to a different k_{max} in the analysis. We show the cases of $k_{\text{max}} = 0.2$ (blue), 0.25 (red), and 0.3 (green) $h \text{ Mpc}^{-1}$ and also show the results of the *Planck* 2018 ΛCDM TT,TE,EE+lowE (gray). The cases of $k_{\text{max}} = 0.25 h \text{ Mpc}^{-1}$ and the *Planck* are identical to those in Figure 3.

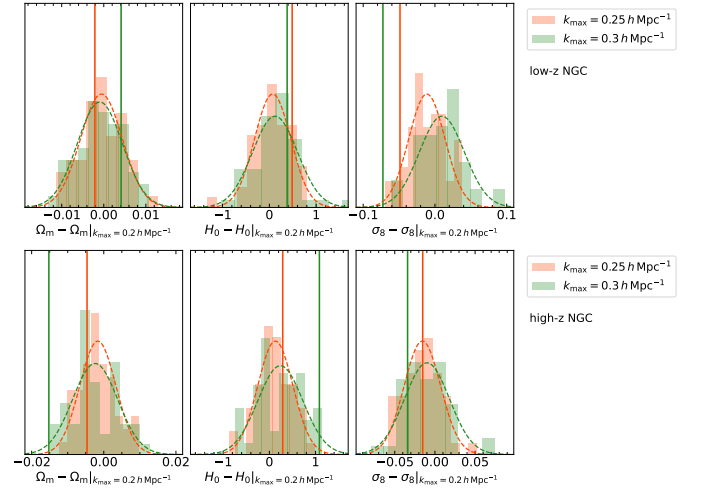


FIG. 9. The distribution of scatters in each cosmological parameter, obtained from the cosmology analysis of noisy mock power spectra for the low- z and high- z NGC samples, using the different k_{max} cuts; the x -axis shows a shift in the MAP value of each parameter at $k_{\text{max}} = 0.25$ or $0.3 h \text{ Mpc}^{-1}$, compared to the MAP value at $k_{\text{max}} = 0.2 h \text{ Mpc}^{-1}$. We used the 50 realizations of the noisy mock spectra, and the histogram in each panel displays the distribution of parameter shifts. The vertical red and green lines denote the shift found from the cosmology analyses of the real BOSS data, shown in Figure 8.

such as the residual shot noise and the HOD parameters are indeed improved by including the information on the higher k . A closer look reveals that the results for $k_{\text{max}} = 0.2$ and $0.25 h \text{ Mpc}^{-1}$ are consistent with each other. However, the result for $k_{\text{max}} = 0.3 h \text{ Mpc}^{-1}$ shows a sizable shift in σ_8 . For the validation tests using the *noiseless* mock signals in Figure 2, we did not find this level of shift in the cosmological parameters.

As a further test of this shift, we use 50 realizations of *noisy* signals that are generated by adding random noise realizations drawn from the BOSS covariance matrix to the *noiseless* mock signals (the mock signals in the right panel of Figure 2). Then we applied the same cosmology analysis pipeline to each of the mock signals to estimate the cosmological parameters. Figure 9 shows the distributions of shifts in the cosmological parameters at $k_{\text{max}} = 0.25$ or $0.30 h \text{ Mpc}^{-1}$ with respect to those at $k_{\text{max}} = 0.20 h \text{ Mpc}^{-1}$, for the low- z and high- z NGC samples which give the dominant contributions to the cosmological constraints of our full analysis. The figure shows that there is a reasonable chance to have the parameter shifts for $k_{\text{max}} = 0.25 h \text{ Mpc}^{-1}$ seen from the actual BOSS data. However, the shifts in some parameters for $k_{\text{max}} = 0.3 h \text{ Mpc}^{-1}$ are at the tail of the distribution of the mock results, indicating a possible hint in the systematic effects at $k \gtrsim 0.25 h \text{ Mpc}^{-1}$, *e.g.*, a limitation of the halo model approach at such high k scales or a residual systematic error in the power spectrum data. Hence our fiducial choice of $k_{\text{max}} = 0.25 h \text{ Mpc}^{-1}$ seems reasonable

against possible systematic effects.

In Appendix D we also study possible effects of the fiber collision and the minimum wavenumber k_{\min} on the cosmological results. Here k_{\min} is the minimum wavenumber in that we include the power spectrum information over $k_{\min} \leq k \leq k_{\max}$ in the cosmological analysis. A brief summary is that these effects do not appear to cause any major systematic effect in our cosmological results.

D. A further test of emulation accuracy

Now we turn to discussion on a possible uncertainty in the model predictions. As discussed in Refs. [38] and [36], our emulator for the redshift-space halo power spectrum is calibrated using a dataset of N -body simulations for the 101 flat w CDM models, where we used 15 realizations for the fiducial *Planck* cosmology and one realization for each of 100 models (more exactly among these we used the data for 80 models as training datasets). Here the 100 models are sampled using the optimal maximum-distance sliced Latin hypercube design in the 6-dimensional parameter space of w CDM cosmology [see 38, for details]. One might think that our emulator has a better accuracy around the *Planck* cosmology, which is different from the MAP model or the model preferred by our cosmology analysis of the BOSS power spectra. To test this possible uncertainty, we ran a new set of N -body simulations for a model near the MAP cosmology in Table III: the model with $\Omega_m = 0.3055$, $H_0 = 68.07 \text{ km s}^{-1} \text{ Mpc}^{-1}$, $\sigma_8 = 0.7650$, and other cosmological parameters are set to the values near to those at MAP. More exactly, we ran each N -body simulation with box side length of $2.5 h^{-1} \text{ Gpc}$ and 3000^3 particles, and use 5 realizations. The total volume is about $78 (h^{-1} \text{ Gpc})^3$, much larger than the BOSS volume ($\sim 5.7 (h^{-1} \text{ Gpc})^3$), so we can sufficiently reduce the sample variance effect in the simulated power spectra. Then we populate galaxies into halos using the same recipe of the halo-galaxy connection used in the Cosmology Challenge paper [35], which is different from our fiducial HOD method. Using the same covariance matrix as we used in the actual cosmology analysis of BOSS data, we perform the same cosmology analysis to the simulated power spectra. This is very similar to the validation test of our method using the simulated power spectrum used in the Cosmology Challenge [35], but this new test gives a validation of our method around the MAP model. Also note that the new set of N -body simulations employs the fixed neutrino mass of 0.06 eV as in the simulations used for the emulator development, while the simulations in the Cosmology Challenges assume zero neutrino mass. Hence, this test also gives a confirmation on the subtle effect of the non-zero neutrino mass, which mainly affects the transfer function of matter density fluctuations. Figure 10 shows that our method recovers each cosmological parameter accurately.

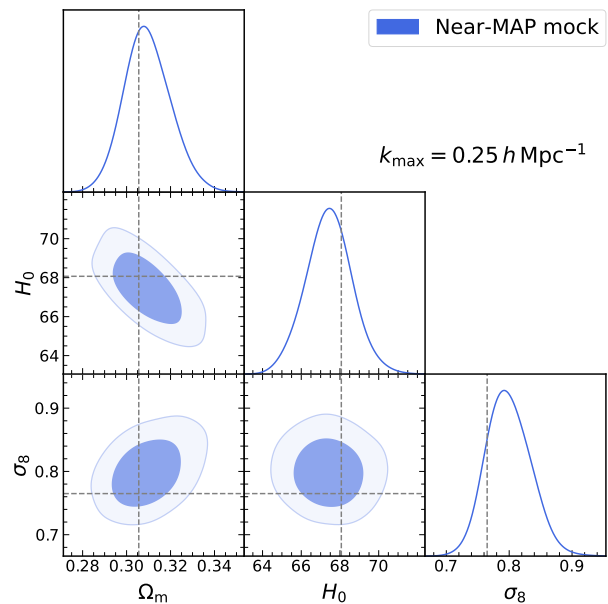


FIG. 10. The posterior distributions of the cosmological parameters using the mock catalogs that are generated from the N -body simulations for a cosmological model that is near to the model at MAP in Table III (see text for details). This is a similar test to Figure 2, and the mock catalogs are generated using the same recipe of halo-galaxy connection as that in the left panel of Figure 2.

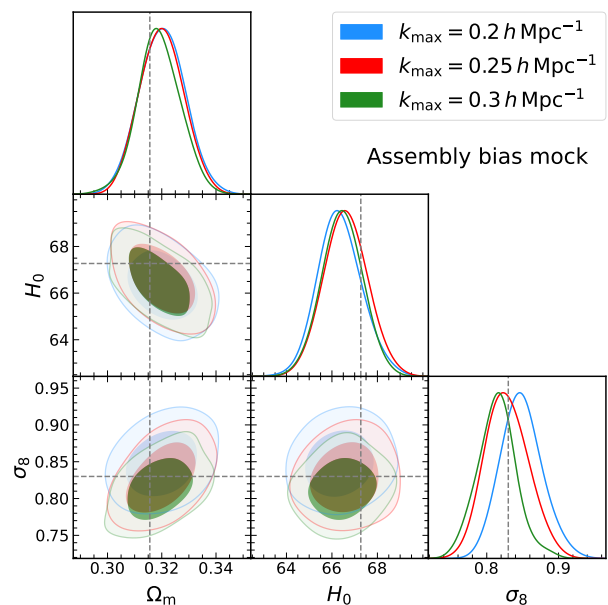


FIG. 11. The posterior distributions of Ω_m , H_0 , and σ_8 , obtained when we apply our analysis pipeline to the mock power spectrum signals that are generated from the mock galaxy catalogs including the assembly bias effect (see text for the details). The mock galaxy catalogs have the same HOD shape as that of the mock catalogs in the right panel of Figure 2, but were generated by populating mock galaxies preferentially into halos that have lower concentrations, in each halo mass bin.

E. Assembly bias

Another concern of the halo model approach is the impact of the “assembly bias” effect; although the simple halo model assumes that the clustering amplitudes of halos (and galaxies) are determined by halo masses, they might depend on a secondary parameter, depending on the assembly history of halos/galaxies [88, 89]. Even in the presence of the assembly bias, the redshift-space distortion effect due to the peculiar velocities are unlikely to be affected by the assembly bias, because the peculiar velocities arise directly from the gravitational field [17]. To test a possible effect of the assembly bias on cosmological analysis, we use the mock catalogs of galaxies including the assembly bias effect in Ref. [17], where galaxies are populated preferentially into halos that have lower concentrations as a proxy of the assembly history [see 17, for details]. The mock catalogs including the assembly bias effect are generated from the same N -body simulations as those used in the right panel of Figure 2; therefore the total volume is about $128 (h^{-1} \text{Gpc})^3$. The mock galaxies have about 30% higher amplitudes in the real-space correlation function at large scales, compared to that of the mock galaxies without the assembly bias effect, which otherwise have the same HOD. We generated the mock signals for each of the BOSS-like galaxy samples, and applied the same pipeline of cosmology analysis to the mock signals. Note that the assembly bias has not been detected with high significance from the BOSS galaxies [*e.g.* 90].

Figure 11 shows the cosmological parameters obtained from the mock catalogs including the assembly bias effect. It can be found that the assembly bias does not cause a significant bias in the inferred cosmological parameters, Ω_m , H_0 and σ_8 . This is consistent with the Fisher forecast in the previous work [17], confirming that the BAO and RSD information are not affected by the assembly bias effect, even after marginalization over the halo-galaxy connection parameters. In other words, the cosmology analysis using the redshift-space power spectrum does not rely on the halo mass estimate. This result is contrasted with that in Ref. [78]: they found that the assembly bias causes a significant bias in the cosmological parameters, especially σ_8 and Ω_m , if a hypothetical joint-probe cosmology analysis using the galaxy-galaxy weak lensing and the projected correlation function is applied to the mock signals including the assembly bias effect. In such a method, the galaxy-galaxy weak lensing plays an important role to constrain the average mass of host halos, which in turn helps determine the galaxy bias uncertainties to obtain the clustering amplitude of matter at large scales. However, the assembly bias disturbs the scaling relation of the large-scale bias amplitude with halo mass, and in turn leads to biases in the inferred cosmological parameters. On the other hand, our method using the redshift-space power spectrum does not rely on the halo mass estimate. Hence we conclude that our cosmological results for the BOSS galaxies are unlikely

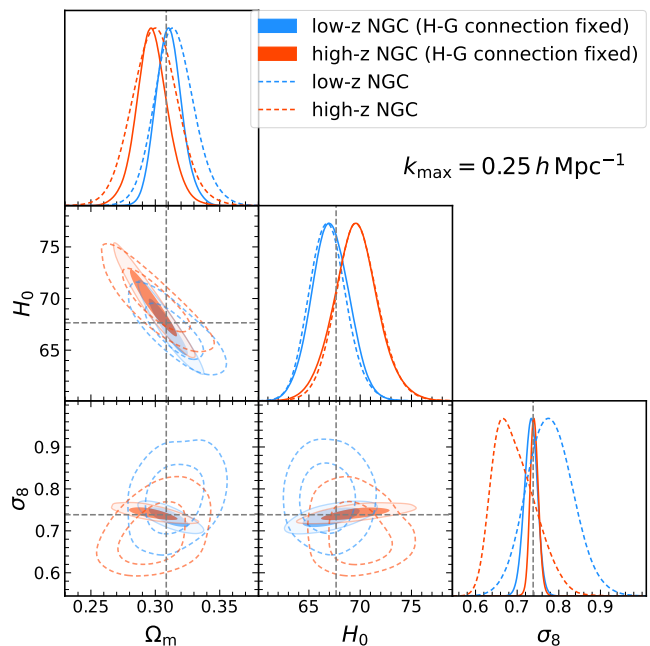


FIG. 12. The posterior distributions of the cosmological parameters, obtained from the cosmology analysis of the real BOSS data for either of the low- z or high- z NGC sample, when fixing the 7 halo-galaxy connection parameters to their values at MAP in Figure 14. The dashed-line contours and 1d posterior distribution are the same as in Figure 14.

affected by the assembly bias, although the impact of more general assembly bias effects on cosmology inference with the redshift-space power spectrum further needs to be studied, *e.g.*, using the results in cosmological hydrodynamical simulations [*e.g.* 91].

F. Impact of uncertainty in the halo-galaxy connection

Finally we comment on the impact of the halo-galaxy connection parameters on the cosmological parameters. We have so far employed broad priors of these nuisance parameters. Other observables such as galaxy-galaxy weak lensing [86, 92] can be used to infer the HOD parameters. Throughout this paper, we have employed a fairly broad prior range for each of 7 halo-galaxy connection parameters. In this subsection, we study how the cosmological parameter estimation can be improved if we have some knowledge on the HOD parameters.

As a working example, in Figure 12 we show the posterior distributions of the cosmological parameters obtained from the BOSS data by fixing the halo-galaxy connection parameters to their values at MAP in our fiducial analysis (the results for Figure 3). Therefore, this can be regarded as the best-case scenario where the halo-galaxy connection of the galaxy sample is perfectly known. The figure shows that the cosmological param-

ters are significantly improved. It is interesting to observe that the level of improvement of the parameter constraint varies with the parameters. We can see that Ω_m and H_0 , which are mostly determined by the geometrical information through the BAO feature and also partly from the spectral shape information, are not significantly improved as compared to σ_8 , which is an amplitude-related parameter. This is telling that the overall amplitude of the cosmological fluctuations is the hardest to interpret from observations due to the strong degeneracy with the galaxy bias uncertainty or the uncertainty in halo-galaxy connection.

VI. CONCLUSION

In this paper, we used an *emulator* of halo clustering statistics to estimate the cosmological parameters from the full-shape analysis of the redshift-space power spectra measured from the BOSS DR12 galaxy catalog over $0.2 < z < 0.75$. Combining with the HOD model, the emulator allows us to compute the redshift-space power spectra of galaxies for a given cosmological model within the flat Λ CDM cosmology, in less than a CPU second. It enables the parameter inference of the BOSS spectra in a multi-dimensional parameter space (33 parameters in this study). We showed that the emulator model well reproduces the monopole, quadrupole and hexadecapole moments of the redshift-space power spectra simultaneously for all of the 4 galaxy subsamples. Our method yields stringent constraints on the cosmological parameters, Ω_m , H_0 and σ_8 , even after marginalization over uncertainties in the nuisance parameters including the halo-galaxy connection parameters: more precisely, $\Omega_m = 0.300 \pm 0.011$, $H_0 = 68.35^{+1.21}_{-1.39} \text{ km s}^{-1} \text{ Mpc}^{-1}$, and $\sigma_8 = 0.742^{+0.035}_{-0.036}$, for the mode and the 68% credible interval of the 1d posterior distribution (Figure 3 and Table III). The cosmological parameters we obtained are consistent with those from the independent studies for the same BOSS spectra using EFTofLSS as the theoretical template [26, 27], even though the theoretical templates are totally different. This shows the robustness of the redshift-space power spectrum method for estimating the cosmological parameters: the BAO, AP effects and RSD information can be robustly extracted as long as the uncertainties in the nonlinear effects and galaxy properties are marginalized over. The statistical precision for each of the main parameters, Ω_m , H_0 and σ_8 is also comparable with that from the EFTofLSS methods. One might think that the halo model could allow us to use the redshift-space power spectra down to a larger k and therefore lead to a more stringent constraint on the parameters, compared to the EFTofLSS method that treats all the galaxy bias parameters as nuisance parameters. However, this is not the case. We think there are a few reasons for this result. First, we employed quite broad priors for each of the HOD parameters and did not include any information on the abun-

dance of galaxies. Hence our analysis might be considered a conservative approach. Second, the power spectrum information at $k \gtrsim 0.2 h \text{ Mpc}^{-1}$ is in the shot noise dominated regime, and the cosmological parameters are not improved even if including the power spectrum information on $k \gtrsim 0.2 h \text{ Mpc}^{-1}$ (Figure 8). Our results are also in good agreement with the *Planck* 2018 results [47] for Ω_m and H_0 , but indicate a slight tension for σ_8 similarly to those reported by the weak lensing analyses [80, 82, 83].

There is a promising route to improving our cosmological constraints. It is a joint-probes cosmology: although we use the redshift-space power spectrum as the data vector in this paper, there is another observable available in the BOSS footprint. The promising one is the galaxy-galaxy weak lensing, which can be obtained by cross-correlating the positions of BOSS galaxies with shapes of background galaxies, where the background galaxies can be taken from an imaging survey overlapping with some portion of the BOSS footprint. For this, the Subaru HSC and some parts of the DES and KiDS surveys have an overlapping region with the BOSS footprints, and the galaxy-galaxy weak lensing can be measured from the joint analysis of BOSS and these imaging surveys. Since the galaxy-galaxy weak lensing can measure the average mass distribution around the BOSS galaxies, it helps observationally disentangle the galaxy bias uncertainty or yields stringent constraints on the HOD parameters in the halo model picture. In fact, Miyatake *et al.* (in prep.) combined the galaxy-galaxy weak lensing, measured from the HSC data of small area coverage 140 sq. degrees, with the *projected* correlation function of BOSS galaxies in the cosmological analysis and then obtained the accuracy of $\sigma(S_8) \simeq 0.05$, compared to our constraint of $\sigma(S_8) \sim 0.04$ although S_8 is not a best parameter to which the redshift-space power spectrum is sensitive. The galaxy-galaxy weak lensing arises mainly from Fourier modes in the two-dimensional space perpendicular to the line-of-sight direction, and it was shown that it carries almost independent information from the redshift-space power spectrum that arises from Fourier modes in the three-dimensional space [93]. Hence, combining the redshift-space power spectrum with the galaxy-galaxy weak lensing helps disentangle the degeneracy between the galaxy bias uncertainty (the halo-galaxy connection) and the cosmological parameters, leading to an improved estimation of the cosmological parameters (see Figure 12 for a possible improvement in the best-case scenario). To do this, our emulator based method easily enables to jointly combine the two observables in the same halo model framework for parameter inference. This is definitely an interesting direction, and will be our future work.

ACKNOWLEDGMENTS

We thank Mikhail Ivanov, Oliver Philcox, Shun Saito, Masato Shirasaki, Marko Simonović,

Naonori S. Sugiyama, Sunao Sugiyama, Ryuichi Takahashi, Digvijay Wadekar, and Matias Zaldarriaga for useful discussions. Y.K. also thanks to the Yukawa Institute for Theoretical Physics, Kyoto University for the warm hospitality where this work was partly done. This work was supported in part by World Premier International Research Center Initiative, MEXT, Japan, and JSPS KAKENHI Grant No. JP15H03654, JP15H05887, JP15H05893, JP15K21733, JP17H01131, JP17K14273, JP19H00677, JP20H04723, JP20H05850, JP20H05861, JP20H05855, and JP21H01081, by Japan Science and Technology Agency (JST) CREST JPMHCR1414, by JST AIP Acceleration Research Grant No. JP20317829, Japan, and by Basic Research Grant (Super AI) of Institute for AI and Beyond of the University of Tokyo. Y.K. was also supported by the Advanced Leading Graduate Course for Photon Science at the University of Tokyo. The N -body simulations and subsequent halo-catalog creation in the DARK QUEST simulation suite used in this work were carried out on Cray XC50 at Center for Computational Astrophysics, National Astronomical Observatory of Japan.

Appendix A: Survey window function

We make a detailed description on the implementation of the survey window function used in this work. Since our emulator supports only the wavenumber range $k < 0.6 h \text{ Mpc}^{-1}$, we employ the method using the multipole moments of the Fourier-space window function proposed in Ref. [24]:

$$\begin{aligned} \left| \tilde{W}(k, k') \right|_{\ell L}^2 &= 2i^\ell (-i)^L (2\ell + 1) \\ &\times \sum_{i \neq j}^{N_{\text{ran}}} w(\mathbf{x}_i) w(\mathbf{x}_j) j_\ell(k|\mathbf{s}|) j_L(k'|\mathbf{s}|) \mathcal{L}_\ell(\hat{\mathbf{x}}_h \cdot \hat{\mathbf{s}}) \mathcal{L}_L(\hat{\mathbf{x}}_h \cdot \hat{\mathbf{s}}), \end{aligned} \quad (\text{A1})$$

where $w(\mathbf{x}_i) = \bar{n}_g^w(\mathbf{x}_i) = \bar{n}_g(z_i) w_{\text{FKP},i}$ and $\mathbf{s} = \mathbf{x}_j - \mathbf{x}_i$, $\mathbf{x}_h = (\mathbf{x}_i + \mathbf{x}_j)/2$ for each pair of random particles. This formula can be rewritten as

$$\begin{aligned} \left| \tilde{W}(k, k') \right|_{\ell L}^2 &= 2i^\ell (-i)^L (2\ell + 1) \times \\ &\int_0^\infty ds \int_{-1}^1 \frac{d\mu_s}{2} W^2(s, \mu_s) j_\ell(k s \mu_s) j_L(k' s \mu_s) \mathcal{L}_\ell(\mu_s) \mathcal{L}_L(\mu_s), \end{aligned} \quad (\text{A2})$$

where we define the configuration-space window function:

$$W^2(s, \mu_s) \approx \sum_{i \neq j}^{N_{\text{ran}}} w(\mathbf{x}_i) w(\mathbf{x}_j) |_{s=|\mathbf{s}|, \mu_s=\hat{\mathbf{x}}_h \cdot \hat{\mathbf{s}}}. \quad (\text{A3})$$

To compute the window function above, we use the publicly available multipole moments of the BOSS DR12

configuration-space window function,

$$\begin{aligned} W_\ell^2(s) &= \frac{2\ell + 1}{2} \int_{-1}^1 d\mu_s W^2(s, \mu_s) \mathcal{L}_\ell(\mu_s) \\ &\propto \sum_{i \neq j}^{N_{\text{ran}}} w(\mathbf{x}_i) w(\mathbf{x}_j) \mathcal{L}_\ell(\hat{\mathbf{x}}_h \cdot \hat{\mathbf{s}}) |_{s=|\mathbf{s}|}, \end{aligned} \quad (\text{A4})$$

where we normalize these functions so that $W_0^2(s=0) = 1$. We approximate $W^2(s, \mu_s)$ by

$$W^2(s, \mu_s) \simeq \sum_{\ell=0,2,4,6,8} W_\ell^2(s) \mathcal{L}_\ell(\mu_s), \quad (\text{A5})$$

and substitute it into Eq. (A2).

Appendix B: Posterior distributions of the halo-galaxy connection parameters in the validation test

Figure 13 show the posterior distributions of the halo-galaxy connection parameters, obtained from the cosmology analysis of the mock data vector that are generated from the mock catalogs of BOSS-like galaxies. The mock galaxy catalog is the same as that used in the right panel of Figure 2. The figure shows that some of the halo-galaxy connection parameters are not necessarily well recovered, although the cosmological parameters are fairly well recovered as shown in Figure 2. The size of the posterior contours for the halo-galaxy connection parameters indeed shrinks with including the power spectrum information on the higher k .

Appendix C: Posterior distributions in full parameter space

For comprehensiveness of our discussion, in Figure 14 we show the posterior distributions in each 2d subspace of the full parameters for the Λ CDM model for each galaxy sample, based on our baseline analysis setup (Table II).

Appendix D: Tests of the fiber collision effect and the minimum wavenumber k_{min}

Next we investigate the impact of the fiber collision on the cosmological parameter inference from the redshift-space galaxy power spectrum. The fiber collision, which occurs due to the inability of the two adjacent optical fibers to be closer than some finite separation angle, is a potential systematic effect on the cosmological parameter inference. The likelihood of the fiber collision depends on the number density of target galaxies on the celestial sphere, and it leads to an anisotropic effect in the measured power spectrum. Ref. [94] shows that the correction to the fiber collision effect on the galaxy power

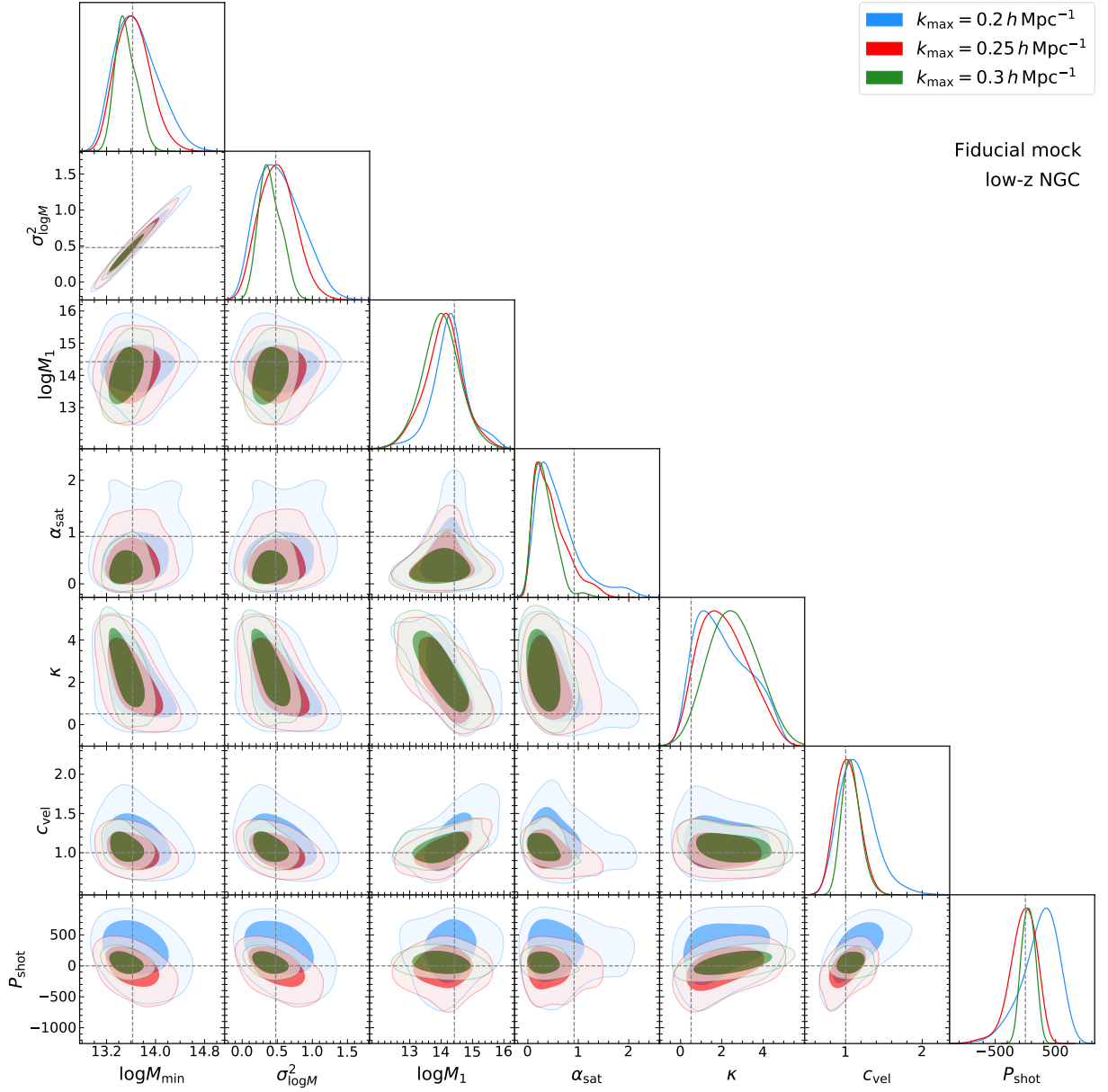


FIG. 13. The posterior distributions of the galaxy-halo connection parameters, for the low- z NGC sample as an example, obtained from the combined analysis using the mock catalogs that are generated using the same HOD model as in our theoretical template (the right panel of Figure 2). The dashed lines in each plot denote the input value of each parameter that is used when generating the mock galaxy catalogs.

spectrum depends on the true power spectrum itself, and suggests the way for the correction. In this work, instead of implementing the correction in the model prediction, we examine the extent to which the fiber collisions affect the cosmology inference.

Figure 15 shows a comparison of the parameter inference between the cases of with/without the fiber collisions. To investigate the influence of the fiber collisions on the cosmological parameter inference, we use the PATCHY mocks which have the fiber collision weights. The fiber collision weights in the PATCHY mocks are assigned following Ref. [58], which reflects the nearest

neighbor (NN) method in Ref. [95]. In this figure we see that there are only marginal differences in the parameter posteriors between the case with the fiber collisions corrected by the NN weights (empty, dashed line contours) and that of the true power spectrum with no fiber collisions (filled, solid line contours), for both the low- z and high- z NGCs, up to $k_{\text{max}} = 0.3 h \text{ Mpc}^{-1}$. Hence we conclude that the fiber collision effect has no significant impact on the cosmology analysis.

We mention the influence of the minimum wavenumber k_{min} of the power spectrum signals we use in the cosmological inference. Figure 16 shows the param-

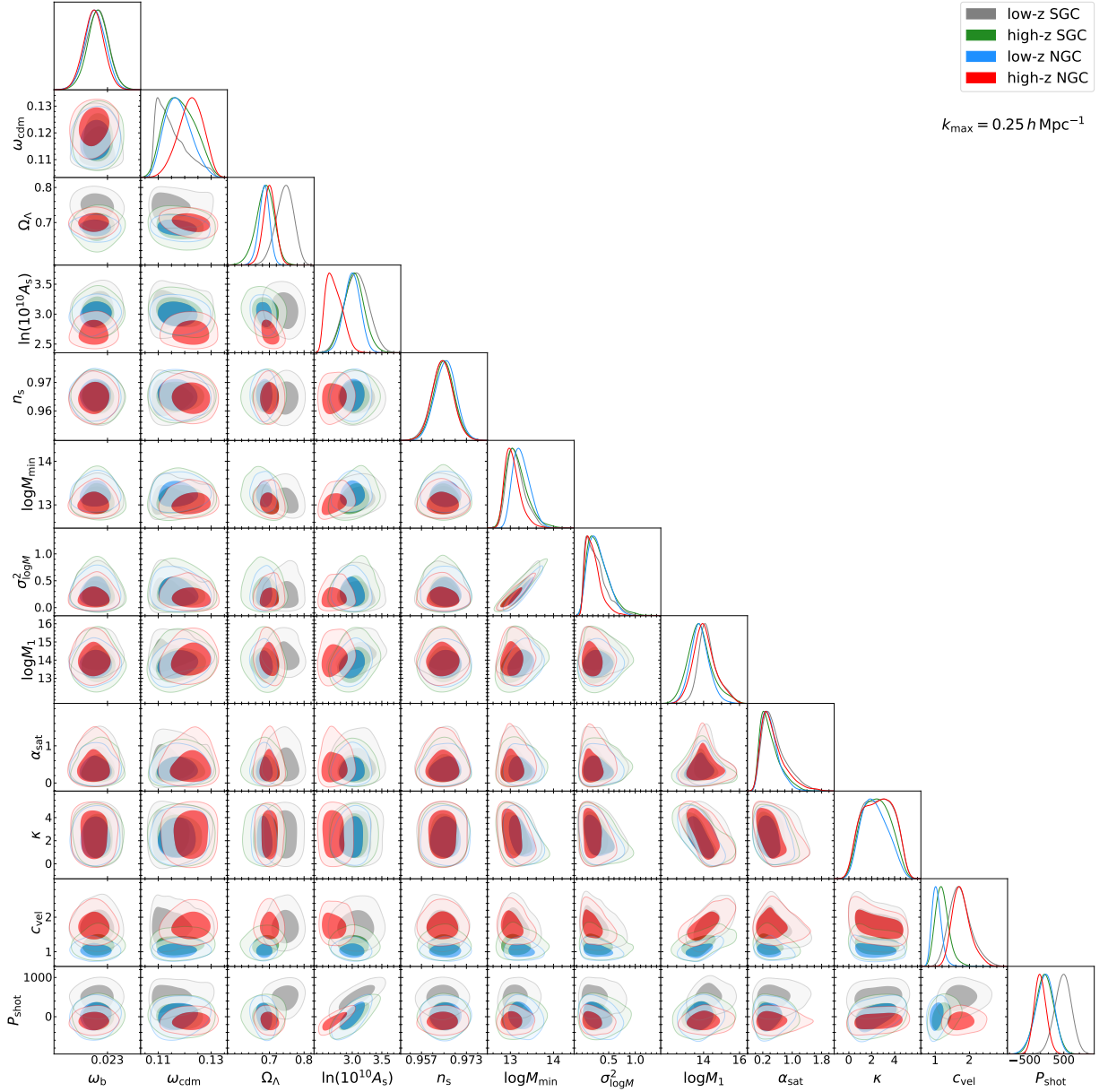


FIG. 14. The posterior distributions in each 2d subspace of the full parameters for each of the 4 galaxy samples, for the cosmology analysis in Figure 3: the low- z NGC, low- z SGC, high- z NGC and high- z SGC samples, respectively. The posterior distributions are from the joint parameter inference of these parameters (33 parameters in total as given in Table II): 5 cosmological parameters (while we impose tight Gaussian priors to ω_b and n_s) and each sample is characterized by 7 nuisance parameters (5 HOD parameters, the virial velocity parameter, and the residual shot noise parameter).

eter inference results for different values of $k_{\min} = 0.005, 0.02$, and $0.05 h \text{ Mpc}^{-1}$ while we keep $k_{\max} = 0.25 h \text{ Mpc}^{-1}$. Here $k_{\min} = 0.005 h \text{ Mpc}^{-1}$ is our default

choice throughout this paper. It shows that the choice of k_{\min} has no significant effect on the cosmological parameter inference.

[1] Shaun Cole, Will J. Percival, John A. Peacock, Peder Norberg, Carlton M. Baugh, Carlos S. Frenk, Ivan Baldry, Joss Bland-Hawthorn, Terry Bridges, Russell Cannon, Matthew Colless, Chris Collins, Warrick Couch,

Nicholas J. G. Cross, Gavin Dalton, Vincent R. Eke, Roberto De Propris, Simon P. Driver, George Efstathiou, Richard S. Ellis, Karl Glazebrook, Carole Jackson, Adrian Jenkins, Ofer Lahav, Ian Lewis, Stuart

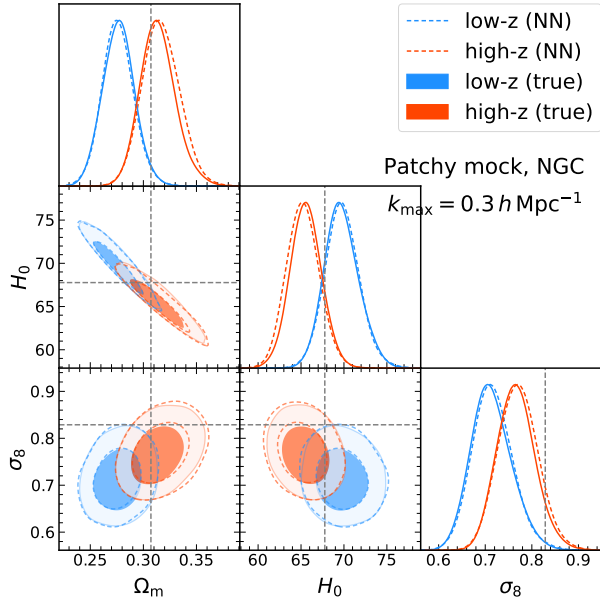


FIG. 15. The comparison of the cosmological parameter inferences between the PATCHY mock power spectra with and without the fiber collisions. We show the cases of the low- z (blue) and high- z (red) NGCs and $k_{\max} = 0.3 h \text{ Mpc}^{-1}$. The empty dashed-line contours are the results for the PATCHY mocks where we include the fiber collision weights. The filled solid-line contours are those for the same mocks where we assume all of the fiber collision weights are unity, *i.e.*, no fiber collisions. The gray horizontal and vertical dashed lines indicate the input cosmological parameter values used in the simulations from which the PATCHY mocks are created.

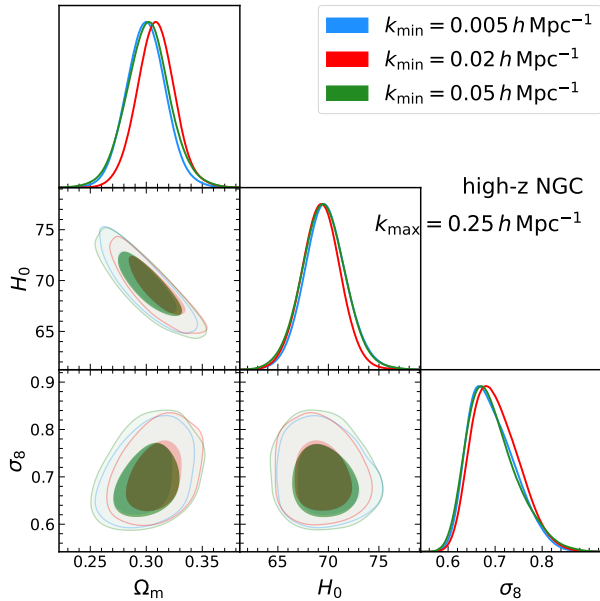


FIG. 16. The dependence of the cosmological parameter constraints on the minimum wavenumber k_{\min} used in the analysis. We tested on the high- z NGC sample of the BOSS data and the cases of $k_{\min} = 0.005$ (our fiducial setting, blue), 0.002 (red) and $0.05 h \text{ Mpc}^{-1}$ (green), while fixing $k_{\max} = 0.25 h \text{ Mpc}^{-1}$.

Lumsden, Steve Maddox, Darren Madgwick, Bruce A. Peterson, Will Sutherland, and Keith Taylor. The 2dF Galaxy Redshift Survey: power-spectrum analysis of the final data set and cosmological implications. *Monthly Notices of the Royal Astronomical Society*, 362(2):505–534, September 2005.

- [2] Daniel J. Eisenstein, Idit Zehavi, David W. Hogg, Roman Scoccimarro, Michael R. Blanton, Robert C. Nichol, Ryan Scranton, Hee-Jong Seo, Max Tegmark, Zheng Zheng, Scott F. Anderson, Jim Annis, Neta Bahcall, Jon Brinkmann, Scott Burles, Francisco J. Castander, Andrew Connolly, Istvan Csabai, Mamoru Doi, Masataka Fukugita, Joshua A. Frieman, Karl Glazebrook, James E. Gunn, John S. Hendry, Gregory Hennessy, Zeljko Ivezić, Stephen Kent, Gillian R. Knapp, Huan Lin, Yeong-Shang Loh, Robert H. Lupton, Bruce Margon, Timothy A. McKay, Avery Meiksin, Jeffery A. Munn, Adrian Pope, Michael W. Richmond, David Schlegel, Donald P. Schneider, Kazuhiro Shimasaku, Christopher Stoughton, Michael A. Strauss, Mark SubbaRao, Alexander S. Szalay, István Szapudi, Douglas L. Tucker, Brian Yanny, and Donald G. York. Detection of the Baryon Acoustic Peak in the Large-Scale Correlation Function of SDSS Luminous Red Galaxies. *The Astrophysical Journal*, 633(2):560–574, November 2005.
- [3] Teppei Okumura, Takahiko Matsubara, Daniel J. Eisenstein, Issha Kayo, Chiaki Hikage, Alexander S. Szalay, and Donald P. Schneider. Large-Scale Anisotropic Correlation Function of SDSS Luminous Red Galaxies. *The Astrophysical Journal*, 676(2):889–898, April 2008.
- [4] David Parkinson, Signe Riemer-Sørensen, Chris Blake, Gregory B. Poole, Tamara M. Davis, Sarah Brough, Matthew Colless, Carlos Contreras, Warrick Couch, Scott Croom, Darren Croton, Michael J. Drinkwater, Karl Forster, David Gilbank, Mike Gladders, Karl Glazebrook, Ben Jelliffe, Russell J. Jurek, I. hui Li, Barry Madore, D. Christopher Martin, Kevin Pimbblet, Michael Pracy, Rob Sharp, Emily Wisnioski, David Woods, Ted K. Wyder, and H. K. C. Yee. The WiggleZ Dark Energy Survey: Final data release and cosmological results. *Phys. Rev. D*, 86(10):103518, November 2012.
- [5] Shadab Alam, Metin Ata, Stephen Bailey, Florian Beutler, Dmitry Bizyaev, Jonathan A. Blazek, Adam S. Bolton, Joel R. Brownstein, Angela Burden, Chia-Hsun Chuang, Johan Comparat, Antonio J. Cuesta, Kyle S. Dawson, Daniel J. Eisenstein, Stephanie Escoffier, Héctor Gil-Marín, Jan Niklas Grieb, Nick Hand, Shirley Ho, Karen Kinemuchi, David Kirkby, Francisco Kitaura, Elena Malanushenko, Viktor Malanushenko, Claudia Maraston, Cameron K. McBride, Robert C. Nichol, Matthew D. Olmstead, Daniel Oravetz, Nikhil Padmanabhan, Nathalie Palanque-Delabrouille, Kaike Pan, Marcos Pellejero-Ibanez, Will J. Percival, Patrick Petitjean, Francisco Prada, Adrian M. Price-Whelan, Beth A. Reid, Sergio A. Rodríguez-Torres, Natalie A. Roe, Ashley J. Ross, Nicholas P. Ross, Graziano Rossi, Jose Alberto Rubiño-Martín, Shun Saito, Salvador Salazar-Albornoz, Lado Samushia, Ariel G. Sánchez, Siddharth Satpathy, David J. Schlegel, Donald P. Schneider, Claudia G. Scóccola, Hee-Jong Seo, Erin S. Sheldon, Audrey Simmons, Anže Slosar, Michael A. Strauss, Molly E. C. Swanson, Daniel Thomas, Jeremy L. Tinker, Rita Tojeiro, Mariana Vargas Magaña, Jose Alberto Vazquez, Licia Verde, David A. Wake, Yuting Wang,

- David H. Weinberg, Martin White, W. Michael Wood-Vasey, Christophe Yèche, Idit Zehavi, Zhongxu Zhai, and Gong-Bo Zhao. The clustering of galaxies in the completed SDSS-III Baryon Oscillation Spectroscopic Survey: cosmological analysis of the DR12 galaxy sample. *Monthly Notices of the Royal Astronomical Society*, 470(3):2617–2652, Sep 2017.
- [6] Teppei Okumura, Chiaki Hikage, Tomonori Totani, Motonari Tōnegawa, Hiroyuki Okada, Karl Glazebrook, Chris Blake, Pedro G. Ferreira, Surhud More, Atsushi Taruya, Shinji Tsujikawa, Masayuki Akiyama, Gavin Dalton, Tomotsugu Goto, Takashi Ishikawa, Fumihide Iwamuro, Takahiko Matsubara, Takahiro Nishimichi, Kouji Ohta, Ikkoh Shimizu, Ryuichi Takahashi, Naruhisa Takato, Naoyuki Tamura, Kiyoto Yabe, and Naoki Yoshida. The Subaru FMOS galaxy redshift survey (Fast-Sound). IV. New constraint on gravity theory from redshift space distortions at $z \sim 1.4$. *Publ. Astron. Soc. Japan*, 68(3):38, June 2016.
- [7] Shadab Alam, Marie Aubert, Santiago Avila, Christophe Balland, Julian E. Bautista, Matthew A. Bershad, Dmitry Bizyaev, Michael R. Blanton, Adam S. Bolton, Jo Bovy, Jonathan Brinkmann, Joel R. Brownstein, Etienne Burtin, Solène Chabanier, Michael J. Chapman, Peter Doohyun Choi, Chia-Hsun Chuang, Johan Comparat, Marie-Claude Cousinou, Andrei Cuceu, Kyle S. Dawson, Sylvain de la Torre, Arnaud de Mattia, Victoria de Sainte Agathe, Hélion du Mas des Bourboux, Stephanie Escoffier, Thomas Etourneau, James Farr, Andreu Font-Ribera, Peter M. Frinchaboy, Sebastien Fromenteau, Héctor Gil-Marín, Jean-Marc Le Goff, Alma X. Gonzalez-Morales, Violeta Gonzalez-Perez, Kathleen Grabowski, Julien Guy, Adam J. Hawken, Jiamin Hou, Hui Kong, James Parker, Mark Klaene, Jean-Paul Kneib, Sicheng Lin, Daniel Long, Brad W. Lyke, Axel de la Macorra, Paul Martini, Karen Masters, Faizan G. Mohammad, Jeongin Moon, Eva-Maria Mueller, Andrea Muñoz-Gutiérrez, Adam D. Myers, Seshadri Nadathur, Richard Neveux, Jeffrey A. Newman, Pasquier Noterdaeme, Audrey Oravetz, Daniel Oravetz, Nathalie Palanque-Delabrouille, Kaike Pan, Romain Paviot, Will J. Percival, Ignasi Pérez-Ràfols, Patrick Petitjean, Matthew M. Pieri, Abhishek Prakash, Anand Raichoor, Corentin Ravoux, Mehdi Rezaie, James Rich, Ashley J. Ross, Graziano Rossi, Rossana Ruggeri, Vanina Ruhlmann-Kleider, Ariel G. Sánchez, F. Javier Sánchez, José R. Sánchez-Gallego, Conor Sayres, Donald P. Schneider, Hee-Jong Seo, Arman Shafieloo, Anže Slosar, Alex Smith, Julianna Stermer, Amelie Tamone, Jeremy L. Tinker, Rita Tojeiro, Mariana Vargas-Magaña, Andrei Variu, Yuting Wang, Benjamin A. Weaver, Anne-Marie Weijmans, Christophe Yèche, Pauline Zarrouk, Cheng Zhao, Gong-Bo Zhao, and Zheng Zheng. Completed SDSS-IV extended Baryon Oscillation Spectroscopic Survey: Cosmological implications from two decades of spectroscopic surveys at the Apache Point Observatory. *Phys. Rev. D*, 103(8):083533, April 2021.
- [8] Kyle S. Dawson, David J. Schlegel, Christopher P. Ahn, Scott F. Anderson, Éric Aubourg, Stephen Bailey, Robert H. Barkhouser, Julian E. Bautista, Alessandra Beifiori, Andreas A. Berlind, Vaishali Bhardwaj, Dmitry Bizyaev, Cullen H. Blake, Michael R. Blanton, Michael Blomqvist, Adam S. Bolton, Arnaud Borde, Jo Bovy, W. N. Brandt, Howard Brewington, Jon Brinkmann, Peter J. Brown, Joel R. Brownstein, Kevin Bundy, N. G. Busca, William Carithers, Aurelio R. Carnero, Michael A. Carr, Yanmei Chen, Johan Comparat, Natalia Connolly, Frances Cope, Rupert A. C. Croft, Antonio J. Cuesta, Luiz N. da Costa, James R. A. Davenport, Timothée Delubac, Roland de Putter, Saurav Dhital, Anne Ealet, Garrett L. Ebelke, Daniel J. Eisenstein, S. Escoffier, Xiaohui Fan, N. Filiz Ak, Hayley Finley, Andreu Font-Ribera, R. Génova-Santos, James E. Gunn, Hong Guo, Daryl Haggard, Patrick B. Hall, Jean-Christophe Hamilton, Ben Harris, David W. Harris, Shirley Ho, David W. Hogg, Diana Holder, Klaus Honscheid, Joe Huehnerhoff, Beatrice Jordan, Wendell P. Jordan, Guinevere Kauffmann, Eyal A. Kazin, David Kirkby, Mark A. Klaene, Jean-Paul Kneib, Jean-Marc Le Goff, Khee-Gan Lee, Daniel C. Long, Craig P. Loomis, Britt Lundgren, Robert H. Lupton, Marcio A. G. Maia, Martin Makler, Elena Malanushenko, Viktor Malanushenko, Rachel Mandelbaum, Marc Manera, Claudia Maraston, Daniel Margala, Karen L. Masters, Cameron K. McBride, Patrick McDonald, Ian D. McGreer, Richard G. McMahon, Olga Mena, Jordi Miralda-Escudé, Antonio D. Montero-Dorta, Francesco Montesano, Demitri Muna, Adam D. Myers, Tracy Naugle, Robert C. Nichol, Pasquier Noterdaeme, Sebastián E. Nuza, Matthew D. Olmstead, Audrey Oravetz, Daniel J. Oravetz, Russell Owen, Nikhil Padmanabhan, Nathalie Palanque-Delabrouille, Kaike Pan, John K. Parejko, Isabelle Pâris, Will J. Percival, Ismael Pérez-Fournon, Ignasi Pérez-Ràfols, Patrick Petitjean, Robert Pfaffenberger, Janine Pforr, Matthew M. Pieri, Francisco Prada, Adrian M. Price-Whelan, M. Jordan Raddick, Rafael Rebolo, James Rich, Gordon T. Richards, Constance M. Rockosi, Natalie A. Roe, Ashley J. Ross, Nicholas P. Ross, Graziano Rossi, J. A. Rubiño-Martin, Lado Samushia, Ariel G. Sánchez, Conor Sayres, Sarah J. Schmidt, Donald P. Schneider, C. G. Scóccola, Hee-Jong Seo, Alaina Shelden, Erin Sheldon, Yue Shen, Yiping Shu, Anže Slosar, Stephen A. Smeed, Stephanie A. Snedden, Fritz Stauffer, Oliver Steele, Michael A. Strauss, Alina Streblyanska, Nao Suzuki, Molly E. C. Swanson, Tomer Tal, Masayuki Tanaka, Daniel Thomas, Jeremy L. Tinker, Rita Tojeiro, Christy A. Tremonti, M. Vargas Magaña, Licia Verde, Matteo Viel, David A. Wake, Mike Watson, Benjamin A. Weaver, David H. Weinberg, Benjamin J. Weiner, Andrew A. West, Martin White, W. M. Wood-Vasey, Christophe Yèche, Idit Zehavi, Gong-Bo Zhao, and Zheng Zheng. The Baryon Oscillation Spectroscopic Survey of SDSS-III. *The Astronomical Journal*, 145:10, Jan 2013.
- [9] Kyle S. Dawson, Jean-Paul Kneib, Will J. Percival, Shadab Alam, Franco D. Albareti, Scott F. Anderson, Eric Armengaud, Éric Aubourg, Stephen Bailey, Julian E. Bautista, Andreas A. Berlind, Matthew A. Bershad, Florian Beutler, Dmitry Bizyaev, Michael R. Blanton, Michael Blomqvist, Adam S. Bolton, Jo Bovy, W. N. Brandt, Jon Brinkmann, Joel R. Brownstein, Etienne Burtin, N. G. Busca, Zheng Cai, Chia-Hsun Chuang, Nicolas Clerc, Johan Comparat, Frances Cope, Rupert A. C. Croft, Irene Cruz-Gonzalez, Luiz N. da Costa, Marie-Claude Cousinou, Jeremy Darling, Axel de la Macorra, Sylvain de la Torre, Timothée Delubac, Hélion du Mas des Bourboux, Tom Dwelly, Anne Ealet,

- Daniel J. Eisenstein, Michael Eracleous, S. Escoffier, Xiaohui Fan, Alexis Finoguenov, Andreu Font-Ribera, Peter Frinchaboy, Patrick Gaulme, Antonis Georgakakis, Paul Green, Hong Guo, Julien Guy, Shirley Ho, Diana Holder, Joe Huehnerhoff, Timothy Hutchinson, Yipeng Jing, Eric Jullo, Vikrant Kamble, Karen Kinemuchi, David Kirkby, Francisco-Shu Kitaura, Mark A. Klaene, Russ R. Laher, Dustin Lang, Pierre Laurent, Jean-Marc Le Goff, Cheng Li, Yu Liang, Marcos Lima, Qiufan Lin, Weipeng Lin, Yen-Ting Lin, Daniel C. Long, Britt Lundgren, Nicholas MacDonald, Marcio Antonio Geimba Maia, Elena Malanushenko, Viktor Malanushenko, Vivek Mariappan, Cameron K. McBride, Ian D. McGreer, Brice Ménard, Andrea Merloni, Andres Meza, Antonio D. Montero-Dorta, Demitri Muna, Adam D. Myers, Kirpal Nandra, Tracy Naugle, Jeffrey A. Newman, Pasquier Noterdaeme, Peter Nugent, Ricardo Ogando, Matthew D. Olmstead, Audrey Oravetz, Daniel J. Oravetz, Nikhil Padmanabhan, Nathalie Palanque-Delabrouille, Kaike Pan, John K. Parejko, Isabelle Pâris, John A. Peacock, Patrick Petitjean, Matthew M. Pieri, Alice Pisani, Francisco Prada, Abhishek Prakash, Anand Raichoor, Beth Reid, James Rich, Jethro Ridd, Sergio Rodriguez-Torres, Aurelio Carnero Rosell, Ashley J. Ross, Graziano Rossi, John Ruan, Mara Salvato, Conor Sayres, Donald P. Schneider, David J. Schlegel, Uros Seljak, Hee-Jong Seo, Branimir Sesar, Sarah Shandera, Yiping Shu, Anže Slosar, Flavia Sobreira, Alina Streblyanska, Nao Suzuki, Donna Taylor, Charling Tao, Jeremy L. Tinker, Rita Tojeiro, Mariana Vargas-Magaña, Yuting Wang, Benjamin A. Weaver, David H. Weinberg, Martin White, W. M. Wood-Vasey, Christophe Yèche, Zhongxu Zhai, Cheng Zhao, Gong-bo Zhao, Zheng Zheng, Guangtun Ben Zhu, and Hu Zou. The SDSS-IV Extended Baryon Oscillation Spectroscopic Survey: Overview and Early Data. *The Astronomical Journal*, 151(2):44, Feb 2016.
- [10] Masahiro Takada, Richard S. Ellis, Masashi Chiba, Jenny E. Greene, Hiroaki Aihara, Nobuo Arimoto, Kevin Bundy, Judith Cohen, Olivier Doré, Genevieve Graves, James E. Gunn, Timothy Heckman, Christopher M. Hirata, Paul Ho, Jean-Paul Kneib, Olivier Le Fèvre, Li-hwai Lin, Surhud More, Hitoshi Murayama, Tohru Nagao, Masami Ouchi, Michael Seiffert, John D. Silverman, Laerte Sodr , David N. Spergel, Michael A. Strauss, Hajime Sugai, Yasushi Suto, Hideki Takami, and Rosemary Wyse. Extragalactic science, cosmology, and Galactic archaeology with the Subaru Prime Focus Spectrograph. *Publ. Astron. Soc. Japan*, 66(1):R1, February 2014.
- [11] Amir Aghamousa et al. The DESI Experiment Part I: Science, Targeting, and Survey Design. 2016.
- [12] R. Laureijs, J. Amiaux, S. Arduini, J. L. Augu res, J. Brinchmann, R. Cole, M. Cropper, C. Dabin, L. Duwet, A. Ealet, B. Garilli, P. Gondoin, L. Guzzo, J. Hoar, H. Hoekstra, R. Holmes, T. Kitching, T. Maciaszek, Y. Mellier, F. Pasian, W. Percival, J. Rhodes, G. Saavedra Criado, M. Sauvage, R. Scaramella, L. Valenziano, S. Warren, R. Bender, F. Castander, A. Cimatti, O. Le F vre, H. Kurki-Suonio, M. Levi, P. Lilje, G. Meylan, R. Nichol, K. Pedersen, V. Popa, R. Rebolo Lopez, H. W. Rix, H. Rottgering, W. Zeilinger, F. Grupp, P. Hudelet, R. Massey, M. Meneghetti, L. Miller, S. Paltani, S. Paulin-Henriksson, S. Pires, C. Saxton, T. Schrabback, G. Seidel, J. Walsh, N. Aghanim, L. Amendola, J. Bartlett, C. Baccigalupi, J. P. Beaulieu, K. Benabed, J. G. Cuby, D. Elbaz, P. Fosalba, G. Gavazzi, A. Helmi, I. Hook, M. Irwin, J. P. Kneib, M. Kunz, F. Mannucci, L. Moscardini, C. Tao, R. Teyssier, J. Weller, G. Zamorani, M. R. Zapatero Osorio, O. Boulade, J. J. Foumond, A. Di Giorgio, P. Guttridge, A. James, M. Kemp, J. Martignac, A. Spencer, D. Walton, T. Bl mchen, C. Bonoli, F. Bortoletto, C. Cerna, L. Corcione, C. Fabron, K. Jahnke, S. Ligori, F. Madrid, L. Martin, G. Morgante, T. Pamlona, E. Prieto, M. Riva, R. Toledo, M. Trifoglio, F. Zerbi, F. Abdalla, M. Douspis, C. Grenet, S. Borgani, R. Bouwens, F. Courbin, J. M. Delouis, P. Dubath, A. Fontana, M. Frailis, A. Grazian, J. Koppenh fer, O. Mansutti, M. Melchior, M. Mignoli, J. Mohr, C. Neissner, K. Noddle, M. Poncet, M. Scodeggio, S. Serrano, N. Shane, J. L. Starck, C. Surace, A. Taylor, G. Verdoes-Kleijn, C. Vuerli, O. R. Williams, A. Zacchei, B. Altieri, I. Escudero Sanz, R. Kohley, T. Oosterbroek, P. Astier, D. Bacon, S. Bardelli, C. Baugh, F. Bellagamba, C. Benoist, D. Bianchi, A. Biviano, E. Branchini, C. Carbone, V. Cardone, D. Clements, S. Colombi, C. Conselice, G. Cresci, N. Deacon, J. Dunlop, C. Fedeli, F. Fontanot, P. Franzetti, C. Giocoli, J. Garcia-Bellido, J. Gow, A. Heavens, P. Hewett, C. Heymans, A. Holland, Z. Huang, O. Ilbert, B. Joachimi, E. Jennings, E. Kerins, A. Kiessling, D. Kirk, R. Kotak, O. Krause, O. Lahav, F. van Leeuwen, J. Lesgourgues, M. Lombardi, M. Magliocchetti, K. Maguire, E. Majerotto, R. Maoli, F. Marulli, S. Maurogordato, H. McCracken, R. McLure, A. Melchiorri, A. Merson, M. Moresco, M. Nonino, P. Norberg, J. Peacock, R. Pello, M. Penny, V. Pettorino, C. Di Porto, L. Pozzetti, C. Quercellini, M. Radovich, A. Rassat, N. Roche, S. Ronayette, E. Rossetti, B. Sartoris, P. Schneider, E. Semboloni, S. Serjeant, F. Simpson, C. Skordis, G. Smadja, S. Smartt, P. Spano, S. Spiro, M. Sullivan, A. Tilquin, R. Trotta, L. Verde, Y. Wang, G. Williger, G. Zhao, J. Zoubian, and E. Zucca. Euclid Definition Study Report. *arXiv e-prints*, page arXiv:1110.3193, October 2011.
- [13] Neil Gehrels and David N. Spergel. Wide-Field InfraRed Survey Telescope (WFIRST) Mission and Synergies with LISA and LIGO-Virgo. *Journal of Physics: Conference Series*, 610(1):012007, 2015.
- [14] Nick Kaiser. Clustering in real space and in redshift space. *Monthly Notices of the Royal Astronomical Society*, 227:1–21, July 1987.
- [15] A. J. S. Hamilton. Measuring Omega and the Real Correlation Function from the Redshift Correlation Function. *The Astrophysical Journal Letters*, 385:L5, January 1992.
- [16] A. J. S. Hamilton. Linear Redshift Distortions: a Review. 231:185, January 1998.
- [17] Yosuke Kobayashi, Takahiro Nishimichi, Masahiro Takada, and Ryuichi Takahashi. Cosmological information content in redshift-space power spectrum of sdss-like galaxies in the quasinonlinear regime up to $k = 0.3 \, h \, \text{mpc}^{-1}$. *Phys. Rev. D*, 101:023510, Jan 2020.
- [18] F. Bernardreau, S. Colombi, E. Gazta aga, and R. Scoccimarro. Large-scale structure of the Universe and cosmological perturbation theory. *Physics Reports*, 367(1-3):1–248, September 2002.
- [19] Vincent Desjacques, Donghui Jeong, and Fabian Schmidt. Large-scale galaxy bias. *Physics Reports*, 733:1–193, February 2018.
- [20] Atsushi Taruya, Takahiro Nishimichi, and Shun Saito.

- Baryon acoustic oscillations in 2D: Modeling redshift-space power spectrum from perturbation theory. *Phys. Rev. D*, 82(6):063522, September 2010.
- [21] Takahiro Nishimichi and Atsushi Taruya. Baryon acoustic oscillations in 2D. II. Redshift-space halo clustering in N-body simulations. *Phys. Rev. D*, 84(4):043526, August 2011.
- [22] Daniel Baumann, Alberto Nicolis, Leonardo Senatore, and Matias Zaldarriaga. Cosmological non-linearities as an effective fluid. *Journal of Cosmology and Astroparticle Physics*, 2012(7):051, July 2012.
- [23] Beth A. Reid, Hee-Jong Seo, Alexie Leauthaud, Jeremy L. Tinker, and Martin White. A 2.5 per cent measurement of the growth rate from small-scale redshift space clustering of SDSS-III CMASS galaxies. *Monthly Notices of the Royal Astronomical Society*, 444(1):476–502, October 2014.
- [24] Florian Beutler, Shun Saito, Hee-Jong Seo, Jon Brinkmann, Kyle S. Dawson, Daniel J. Eisenstein, Andreu Font-Ribera, Shirley Ho, Cameron K. McBride, Francesco Montesano, Will J. Percival, Ashley J. Ross, Nicholas P. Ross, Lado Samushia, David J. Schlegel, Ariel G. Sánchez, Jeremy L. Tinker, and Benjamin A. Weaver. The clustering of galaxies in the SDSS-III Baryon Oscillation Spectroscopic Survey: testing gravity with redshift space distortions using the power spectrum multipoles. *Monthly Notices of the Royal Astronomical Society*, 443(2):1065–1089, 07 2014.
- [25] Florian Beutler et al. The clustering of galaxies in the completed SDSS-III Baryon Oscillation Spectroscopic Survey: Anisotropic galaxy clustering in Fourier-space. *Monthly Notices of the Royal Astronomical Society*, 466(2):2242–2260, 2017.
- [26] Mikhail M. Ivanov, Marko Simonović, and Matias Zaldarriaga. Cosmological parameters from the boss galaxy power spectrum. *Journal of Cosmology and Astroparticle Physics*, 2020(05):042–042, May 2020.
- [27] Guido d’ Amico, Jérôme Gleyzes, Nickolas Kokron, Katarina Markovic, Leonardo Senatore, Pierre Zhang, Florian Beutler, and Héctor Gil-Marín. The cosmological analysis of the sdss/boss data from the effective field theory of large-scale structure. *Journal of Cosmology and Astroparticle Physics*, 2020(05):005–005, May 2020.
- [28] Sebastián Pueblas and Román Scoccimarro. Generation of vorticity and velocity dispersion by orbit crossing. *Physical Review D*, 80(4), Aug 2009.
- [29] Diego Blas, Mathias Garny, and Thomas Konstandin. Cosmological perturbation theory at three-loop order. *Journal of Cosmology and Astroparticle Physics*, 2014(1):010, January 2014.
- [30] Francis Bernardeau, Atsushi Taruya, and Takahiro Nishimichi. Cosmic propagators at two-loop order. *Phys. Rev. D*, 89(2):023502, January 2014.
- [31] Takahiro Nishimichi, Francis Bernardeau, and Atsushi Taruya. Response function of the large-scale structure of the universe to the small scale inhomogeneities. *Physics Letters B*, 762:247–252, November 2016.
- [32] Atsushi Taruya and Stéphane Colombi. Post-collapse perturbation theory in 1D cosmology – beyond shell-crossing. *Monthly Notices of the Royal Astronomical Society*, 470(4):4858–4884, October 2017.
- [33] Shohei Saga, Atsushi Taruya, and Stéphane Colombi. Lagrangian cosmological perturbation theory at shell-crossing. *Physical Review Letters*, 121(24):241302, December 2018.
- [34] Anaëlle Halle, Takahiro Nishimichi, Atsushi Taruya, Stéphane Colombi, and Francis Bernardeau. Power spectrum response of large-scale structure in 1d and in 3d: tests of prescriptions for post-collapse dynamics. *Monthly Notices of the Royal Astronomical Society*, 499(2):1769–1787, Sep 2020.
- [35] Takahiro Nishimichi, Guido D’Amico, Mikhail M. Ivanov, Leonardo Senatore, Marko Simonović, Masahiro Takada, Matias Zaldarriaga, and Pierre Zhang. Blinded challenge for precision cosmology with large-scale structure: Results from effective field theory for the redshift-space galaxy power spectrum. *Physical Review D*, 102(12), Dec 2020.
- [36] Yosuke Kobayashi, Takahiro Nishimichi, Masahiro Takada, Ryuichi Takahashi, and Ken Osato. Accurate emulator for the redshift-space power spectrum of dark matter halos and its application to galaxy power spectrum. *Phys. Rev. D*, 102(6):063504, September 2020.
- [37] Asantha Cooray and Ravi Sheth. Halo models of large scale structure. *Physics Reports*, 372(1):1–129, December 2002.
- [38] Takahiro Nishimichi, Masahiro Takada, Ryuichi Takahashi, Ken Osato, Masato Shirasaki, Taira Oogi, Hironao Miyatake, Masamune Oguri, Ryoma Murata, Yosuke Kobayashi, and Naoki Yoshida. Dark quest. i. fast and accurate emulation of halo clustering statistics and its application to galaxy clustering. *The Astrophysical Journal*, 884(1):29, oct 2019.
- [39] Y. P. Jing, H. J. Mo, and G. Börner. Spatial Correlation Function and Pairwise Velocity Dispersion of Galaxies: Cold Dark Matter Models versus the Las Campanas Survey. *The Astrophysical Journal*, 494:1–12, February 1998.
- [40] Uroš Seljak. Analytic model for galaxy and dark matter clustering. *Monthly Notices of the Royal Astronomical Society*, 318(1):203–213, October 2000.
- [41] J. A. Peacock and R. E. Smith. Halo occupation numbers and galaxy bias. *Monthly Notices of the Royal Astronomical Society*, 318:1144–1156, November 2000.
- [42] Román Scoccimarro, Ravi K. Sheth, Lam Hui, and Bhuvnesh Jain. How Many Galaxies Fit in a Halo? Constraints on Galaxy Formation Efficiency from Spatial Clustering. *The Astrophysical Journal*, 546(1):20–34, January 2001.
- [43] Zheng Zheng, Andreas A. Berlind, David H. Weinberg, Andrew J. Benson, Carlton M. Baugh, Shaun Cole, Romeel Davé, Carlos S. Frenk, Neal Katz, and Cedric G. Lacey. Theoretical Models of the Halo Occupation Distribution: Separating Central and Satellite Galaxies. *The Astrophysical Journal*, 633(2):791–809, November 2005.
- [44] Zheng Zheng, Idit Zehavi, Daniel J. Eisenstein, David H. Weinberg, and Y. P. Jing. Halo Occupation Distribution Modeling of Clustering of Luminous Red Galaxies. *The Astrophysical Journal*, 707(1):554–572, December 2009.
- [45] <https://data.sdss.org/sas/dr12/boss/lss/>.
- [46] Erik Aver, Keith A. Olive, and Evan D. Skillman. The effects of he i $\lambda 10830$ on helium abundance determinations. *Journal of Cosmology and Astroparticle Physics*, 2015(07):011–011, Jul 2015.
- [47] Planck Collaboration, N. Aghanim, Y. Akrami, M. Ashdown, J. Aumont, C. Baccigalupi, M. Ballardini, A. J. Banday, R. B. Barreiro, N. Bartolo, S. Basak, R. Battye, K. Benabed, J. P. Bernard, M. Bersanelli, P. Bielewicz, J. J. Bock, J. R. Bond, J. Borrill, F. R. Bouchet,

- F. Boulanger, M. Bucher, C. Burigana, R. C. Butler, E. Calabrese, J. F. Cardoso, J. Carron, A. Challinor, H. C. Chiang, J. Chluba, L. P. L. Colombo, C. Combet, D. Contreras, B. P. Crill, F. Cuttaia, P. de Bernardis, G. de Zotti, J. Delabrouille, J. M. Delouis, E. Di Valentino, J. M. Diego, O. Doré, M. Douspis, A. Ducout, X. Dupac, S. Dusini, G. Efstathiou, F. Elsner, T. A. Enßlin, H. K. Eriksen, Y. Fantaye, M. Farhang, J. Fergusson, R. Fernandez-Cobos, F. Finelli, F. Forastieri, M. Frailis, A. A. Fraisse, E. Franceschi, A. Frolov, S. Galeotta, S. Galli, K. Ganga, R. T. Génova-Santos, M. Gerbino, T. Ghosh, J. González-Nuevo, K. M. Górski, S. Gratton, A. Gruppuso, J. E. Gudmundsson, J. Hamann, W. Handley, F. K. Hansen, D. Herranz, S. R. Hildebrandt, E. Hivon, Z. Huang, A. H. Jaffe, W. C. Jones, A. Karakci, E. Keihänen, R. Keskitalo, K. Kiiveri, J. Kim, T. S. Kisner, L. Knox, N. Krachmalnicoff, M. Kunz, H. Kurki-Suonio, G. Lagache, J. M. Lamarre, A. Lasenby, M. Lattanzi, C. R. Lawrence, M. Le Jeune, P. Lemos, J. Lesgourgues, F. Levrier, A. Lewis, M. Liguori, P. B. Lilje, M. Lilley, V. Lindholm, M. López-Cañiego, P. M. Lubin, Y. Z. Ma, J. F. Macías-Pérez, G. Maggio, D. Maino, N. Mandolesi, A. Mangilli, A. Marcos-Caballero, M. Maris, P. G. Martin, M. Martinelli, E. Martínez-González, S. Matarrese, N. Mauri, J. D. McEwen, P. R. Meinhold, A. Melchiorri, A. Mennella, M. Migliaccio, M. Milea, S. Mitra, M. A. Miville-Deschênes, D. Molinari, L. Montier, G. Morgante, A. Moss, P. Natoli, H. U. Nørgaard-Nielsen, L. Pagano, D. Paoletti, B. Partridge, G. Patanchon, H. V. Peiris, F. Perrotta, V. Pettorino, F. Piacentini, L. Polastri, G. Polenta, J. L. Puget, J. P. Rachen, M. Reinecke, M. Remazeilles, A. Renzi, G. Rocha, C. Rosset, G. Roudier, J. A. Rubiño-Martín, B. Ruiz-Granados, L. Salvati, M. Sandri, M. Savelainen, D. Scott, E. P. S. Shellard, C. Sirignano, G. Sirri, L. D. Spencer, R. Sunyaev, A. S. Suur-Uski, J. A. Tauber, D. Tavagnacco, M. Tenti, L. Toffolatti, M. Tomasi, T. Trombetti, L. Valenziano, J. Valiviita, B. Van Tent, L. Vibert, P. Vielva, F. Villa, N. Vittorio, B. D. Wandelt, I. K. Wehus, M. White, S. D. M. White, A. Zacchei, and A. Zonca. Planck 2018 results. VI. Cosmological parameters. *Astronomy and Astrophysics*, 641:A6, September 2020.
- [48] Nick Hand, Yin Li, Zachary Slepian, and Uroš Seljak. An optimal fft-based anisotropic power spectrum estimator. *Journal of Cosmology and Astroparticle Physics*, 2017(07):002–002, Jul 2017.
- [49] Beth Reid, Shirley Ho, Nikhil Padmanabhan, Will J. Percival, Jeremy Tinker, Rita Tojeiro, Martin White, Daniel J. Eisenstein, Claudia Maraston, Ashley J. Ross, Ariel G. Sánchez, David Schlegel, Erin Sheldon, Michael A. Strauss, Daniel Thomas, David Wake, Florian Beutler, Dmitry Bizyaev, Adam S. Bolton, Joel R. Brownstein, Chia-Hsun Chuang, Kyle Dawson, Paul Harding, Francisco-Shu Kitaura, Alexie Leauthaud, Karen Masters, Cameron K. McBride, Surhud More, Matthew D. Olmstead, Daniel Oravetz, Sebastián E. Nuza, Kaike Pan, John Parejko, Janine Pforr, Francisco Prada, Sergio Rodríguez-Torres, Salvador Salazar-Albornoz, Lado Samushia, Donald P. Schneider, Claudia G. Scóccola, Audrey Simmons, and Mariana Vargas-Magana. SDSS-III Baryon Oscillation Spectroscopic Survey Data Release 12: galaxy target selection and large-scale structure catalogues. *Monthly Notices of the Royal Astronomical Society*, 455(2):1553–1573, 11 2015.
- [50] Hume A. Feldman, Nick Kaiser, and John A. Peacock. Power-Spectrum Analysis of Three-dimensional Redshift Surveys. *The Astrophysical Journal*, 426:23, May 1994.
- [51] Emiliano Sefusatti, Martin Crocce, Roman Scoccimarro, and Hugh Couchman. Accurate Estimators of Correlation Functions in Fourier Space. *Monthly Notices of the Royal Astronomical Society*, 460(4):3624–3636, 2016.
- [52] Kazuhiro Yamamoto, Masashi Nakamichi, Akinari Kamino, Bruce A. Bassett, and Hiroaki Nishioka. A Measurement of the Quadrupole Power Spectrum in the Clustering of the 2dF QSO Survey. *Publ. Astron. Soc. Japan*, 58:93–102, February 2006.
- [53] Román Scoccimarro. Fast estimators for redshift-space clustering. *Physical Review D*, 92(8), Oct 2015.
- [54] Davide Bianchi, Héctor Gil-Marín, Rossana Ruggeri, and Will J. Percival. Measuring line-of-sight-dependent fourier-space clustering using ffts. *Monthly Notices of the Royal Astronomical Society: Letters*, 453(1):L11–L15, Aug 2015.
- [55] Digvijay Wadekar, Mikhail M. Ivanov, and Roman Scoccimarro. Cosmological constraints from boss with analytic covariance matrices. *Physical Review D*, 102(12), Dec 2020.
- [56] Nick Hand, Yu Feng, Florian Beutler, Yin Li, Chirag Modi, Uroš Seljak, and Zachary Slepian. nboddykit: An open-source, massively parallel toolkit for large-scale structure. *The Astronomical Journal*, 156(4):160, Sep 2018.
- [57] Francisco-Shu Kitaura, Sergio Rodríguez-Torres, Chia-Hsun Chuang, Cheng Zhao, Francisco Prada, Héctor Gil-Marín, Hong Guo, Gustavo Yepes, Anatoly Klypin, Claudia G. Scóccola, and et al. The clustering of galaxies in the sdss-iii baryon oscillation spectroscopic survey: mock galaxy catalogues for the boss final data release. *Monthly Notices of the Royal Astronomical Society*, 456(4):4156–4173, Jan 2016.
- [58] Sergio A. Rodríguez-Torres, Chia-Hsun Chuang, Francisco Prada, Hong Guo, Anatoly Klypin, Peter Behroozi, Chang Hoon Hahn, Johan Comparat, Gustavo Yepes, Antonio D. Montero-Dorta, Joel R. Brownstein, Claudia Maraston, Cameron K. McBride, Jeremy Tinker, Stefan Gottlöber, Ginevra Favole, Yiping Shu, Francisco-Shu Kitaura, Adam Bolton, Román Scoccimarro, Lado Samushia, David Schlegel, Donald P. Schneider, and Daniel Thomas. The clustering of galaxies in the SDSS-III Baryon Oscillation Spectroscopic Survey: modelling the clustering and halo occupation distribution of BOSS CMASS galaxies in the Final Data Release. *Monthly Notices of the Royal Astronomical Society*, 460(2):1173–1187, 04 2016.
- [59] Anatoly Klypin, Gustavo Yepes, Stefan Gottlöber, Francisco Prada, and Steffen Heß. Multidark simulations: the story of dark matter halo concentrations and density profiles. *Monthly Notices of the Royal Astronomical Society*, 457(4):4340–4359, Feb 2016.
- [60] J. Hartlap, P. Simon, and P. Schneider. Why your model parameter confidences might be too optimistic. Unbiased estimation of the inverse covariance matrix. *Astronomy and Astrophysics*, 464(1):399–404, March 2007.
- [61] Julio F. Navarro, Carlos S. Frenk, and Simon D. M. White. The Structure of Cold Dark Matter Halos. *The Astrophysical Journal*, 462:563, May 1996.

- [62] Chiaki Hikage, Masahiro Takada, and David N. Spergel. Using galaxy-galaxy weak lensing measurements to correct the finger of God. *Monthly Notices of the Royal Astronomical Society*, 419(4):3457–3481, February 2012.
- [63] Chiaki Hikage, Rachel Mandelbaum, Masahiro Takada, and David N. Spergel. Where are the Luminous Red Galaxies (LRGs)? Using correlation measurements and lensing to relate LRGs to dark matter haloes. *Monthly Notices of the Royal Astronomical Society*, 435(3):2345–2370, November 2013.
- [64] Benedikt Diemer and Andrey V. Kravtsov. A Universal Model for Halo Concentrations. *The Astrophysical Journal*, 799(1):108, January 2015.
- [65] Benedikt Diemer and Michael Joyce. An accurate physical model for halo concentrations. *The Astrophysical Journal*, 871(2):168, Jan 2019.
- [66] Benedikt Diemer. Colossus: A python toolkit for cosmology, large-scale structure, and dark matter halos. *The Astrophysical Journal Supplement Series*, 239(2):35, Dec 2018.
- [67] C. Alcock and B. Paczynski. An evolution free test for non-zero cosmological constant. *Nature (London)*, 281:358, October 1979.
- [68] Takahiko Matsubara and Yasushi Suto. Cosmological redshift distortion of correlation functions as a probe of the density parameter and the cosmological constant. *The Astrophysical Journal*, 470(1):L1–L5, Oct 1996.
- [69] Ryan J. Cooke, Max Pettini, and Charles C. Steidel. One percent determination of the primordial deuterium abundance. *The Astrophysical Journal*, 855(2):102, Mar 2018.
- [70] Nils Schöneberg, Julien Lesgourgues, and Deanna C. Hooper. The $\text{bao}+\text{bbn}$ take on the hubble tension. *Journal of Cosmology and Astroparticle Physics*, 2019(10):029–029, Oct 2019.
- [71] Nicholas Metropolis and S. Ulam. The monte carlo method. *Journal of the American Statistical Association*, 44(247):335–341, 1949. PMID: 18139350.
- [72] F. Feroz, M. P. Hobson, and M. Bridges. Multinest: an efficient and robust bayesian inference tool for cosmology and particle physics. *Monthly Notices of the Royal Astronomical Society*, 398(4):1601–1614, Oct 2009.
- [73] Aki Vehtari, Andrew Gelman, Daniel Simpson, Bob Carpenter, and Paul-Christian Bürkner. Rank-Normalization, Folding, and Localization: An Improved \hat{R} for Assessing Convergence of MCMC (with Discussion). *Bayesian Analysis*, 16(2):667 – 718, 2021.
- [74] Andrew Gelman and Donald B. Rubin. Inference from Iterative Simulation Using Multiple Sequences. *Statistical Science*, 7(4):457 – 472, 1992.
- [75] Stephen P. Brooks and Andrew Gelman. General methods for monitoring convergence of iterative simulations. *Journal of Computational and Graphical Statistics*, 7(4):434–455, 1998.
- [76] Andrew Gelman, John B. Carlin, Hal S. Stern, David B. Dunson, Aki Vehtari, and Donald B. Rubin. *Bayesian Data Analysis (3rd ed.)*. CRC Press, 2013.
- [77] Oliver H. E. Philcox, Mikhail M. Ivanov, Marko Simonović, and Matias Zaldarriaga. Combining full-shape and BAO analyses of galaxy power spectra: a 1.6% CMB-independent constraint on H_0 . *Journal of Cosmology and Astroparticle Physics*, 2020(5):032, May 2020.
- [78] Hironao Miyatake, Yosuke Kobayashi, Masahiro Takada, Takahiro Nishimichi, Masato Shirasaki, Sunao Sugiyama, Ryuichi Takahashi, Ken Osato, Surhud More, and Youngsoo Park. Cosmological inference from emulator based halo model I: Validation tests with HSC and SDSS mock catalogs. *arXiv e-prints*, page arXiv:2101.00113, December 2020.
- [79] Sunao Sugiyama, Masahiro Takada, Yosuke Kobayashi, Hironao Miyatake, Masato Shirasaki, Takahiro Nishimichi, and Youngsoo Park. Validating a minimal galaxy bias method for cosmological parameter inference using hsc-sdss mock catalogs. *Physical Review D*, 102(8), Oct 2020.
- [80] Chiaki Hikage, Masamune Oguri, Takashi Hamana, Surhud More, Rachel Mandelbaum, Masahiro Takada, Fabian Köhlinger, Hironao Miyatake, Atsushi J. Nishizawa, Hiroaki Aihara, Robert Armstrong, James Bosch, Jean Coupon, Anne Ducout, Paul Ho, Bau-Ching Hsieh, Yutaka Komiyama, François Lanusse, Alexie Leauthaud, Robert H. Lupton, Elinor Medezinski, Sogo Mineo, Shoken Miyama, Satoshi Miyazaki, Ryoma Murata, Hitoshi Murayama, Masato Shirasaki, Cristóbal Sifón, Melanie Simet, Joshua Speagle, David N. Spergel, Michael A. Strauss, Naoshi Sugiyama, Masayuki Tanaka, Yousuke Utsumi, Shiang-Yu Wang, and Yoshihiko Yamada. Cosmology from cosmic shear power spectra with Subaru Hyper Suprime-Cam first-year data. *Publ. Astron. Soc. Japan*, 71(2):43, April 2019.
- [81] Takashi Hamana, Masato Shirasaki, Satoshi Miyazaki, Chiaki Hikage, Masamune Oguri, Surhud More, Robert Armstrong, Alexie Leauthaud, Rachel Mandelbaum, Hironao Miyatake, Atsushi J. Nishizawa, Melanie Simet, Masahiro Takada, Hiroaki Aihara, James Bosch, Yutaka Komiyama, Robert Lupton, Hitoshi Murayama, Michael A. Strauss, and Masayuki Tanaka. Cosmological constraints from cosmic shear two-point correlation functions with HSC survey first-year data. *Publ. Astron. Soc. Japan*, 72(1):16, February 2020.
- [82] T. M. C. Abbott, F. B. Abdalla, A. Alarcon, J. Aleksić, S. Allam, S. Allen, A. Amara, J. Annis, J. Asorey, S. Avila, D. Bacon, E. Balbinot, M. Banerji, N. Banik, W. Barkhouse, M. Baumer, E. Baxter, K. Bechtol, M. R. Becker, A. Benoit-Lévy, B. A. Benson, G. M. Bernstein, E. Bertin, J. Blazek, S. L. Bridle, D. Brooks, D. Brout, E. Buckley-Geer, D. L. Burke, M. T. Busha, A. Campos, D. Capozzi, A. Carnero Rosell, M. Carrasco Kind, J. Carretero, F. J. Castander, R. Cawthon, C. Chang, N. Chen, M. Childress, A. Choi, C. Conselice, R. Crittenden, M. Crocce, C. E. Cunha, C. B. D’Andrea, L. N. da Costa, R. Das, T. M. Davis, C. Davis, J. De Vicente, D. L. DePoy, J. DeRose, S. Desai, H. T. Diehl, J. P. Dietrich, S. Dodelson, P. Doel, A. Drlica-Wagner, T. F. Eifler, A. E. Elliott, F. Elsner, J. Elvin-Poole, J. Estrada, A. E. Evrard, Y. Fang, E. Fernandez, A. Ferté, D. A. Finley, B. Flaugher, P. Fosalba, O. Friedrich, J. Frieman, J. García-Bellido, M. Garcia-Fernandez, M. Gatti, E. Gaztanaga, D. W. Gerdes, T. Giannantonio, M. S. S. Gill, K. Glazebrook, D. A. Goldstein, D. Gruen, R. A. Gruendl, J. Gschwend, G. Gutierrez, S. Hamilton, W. G. Hartley, S. R. Hinton, K. Honscheid, B. Hoyle, D. Huterer, B. Jain, D. J. James, M. Jarvis, T. Jeltama, M. D. Johnson, M. W. G. Johnson, T. Kacprzak, S. Kent, A. G. Kim, A. King, D. Kirk, N. Kokron, A. Kovacs, E. Krause, C. Krawiec, A. Kremin, K. Kuehn, S. Kuhlmann, N. Kuropatkin, F. Lacasa, O. Lahav, T. S. Li, A. R. Liddle, C. Lid-

- man, M. Lima, H. Lin, N. MacCrann, M. A. G. Maia, M. Makler, M. Manera, M. March, J. L. Marshall, P. Martini, R. G. McMahon, P. Melchior, F. Menanteau, R. Miquel, V. Miranda, D. Mudd, J. Muir, A. Möller, E. Neilsen, R. C. Nichol, B. Nord, P. Nugent, R. L. C. Ogando, A. Palmese, J. Peacock, H. V. Peiris, J. Peoples, W. J. Percival, D. Petravick, A. A. Plazas, A. Porredon, J. Prat, A. Pujol, M. M. Rau, A. Refregier, P. M. Ricker, N. Roe, R. P. Rollins, A. K. Romer, A. Roodman, R. Rosenfeld, A. J. Ross, E. Rozo, E. S. Rykoff, M. Sako, A. I. Salvador, S. Samuroff, C. Sánchez, E. Sanchez, B. Santiago, V. Scarpine, R. Schindler, D. Scolnic, L. F. Secco, S. Serrano, I. Sevilla-Noarbe, E. Sheldon, R. C. Smith, M. Smith, J. Smith, M. Soares-Santos, F. Sobreira, E. Suchyta, G. Tarle, D. Thomas, M. A. Troxel, D. L. Tucker, B. E. Tucker, S. A. Uddin, T. N. Varga, P. Vielzeuf, V. Vikram, A. K. Vivas, A. R. Walker, M. Wang, R. H. Wechsler, J. Weller, W. Wester, R. C. Wolf, B. Yanny, F. Yuan, A. Zenteno, B. Zhang, Y. Zhang, J. Zuntz, and Dark Energy Survey Collaboration. Dark Energy Survey year 1 results: Cosmological constraints from galaxy clustering and weak lensing. *Phys. Rev. D*, 98(4):043526, August 2018.
- [83] Catherine Heymans, Tilman Tröster, Marika Asgari, Chris Blake, Hendrik Hildebrandt, Benjamin Joachimi, Konrad Kuijken, Chieh-An Lin, Ariel G. Sánchez, Jan Luca van den Busch, Angus H. Wright, Alexandra Amon, Maciej Bilicki, Jelte de Jong, Martin Crocce, Andrej Dvornik, Thomas Erben, Maria Cristina Fortuna, Fedor Getman, Benjamin Giblin, Karl Glazebrook, Henk Hoekstra, Shahab Joudaki, Arun Kannawadi, Fabian Köhlinger, Chris Lidman, Lance Miller, Nicola R. Napolitano, David Parkinson, Peter Schneider, HuanYuan Shan, Edwin A. Valentijn, Gijs Verdoes Kleijn, and Christian Wolf. KiDS-1000 Cosmology: Multi-probe weak gravitational lensing and spectroscopic galaxy clustering constraints. *Astronomy and Astrophysics*, 646:A140, February 2021.
- [84] Beth A. Reid and David N. Spergel. Constraining the Luminous Red Galaxy Halo Occupation Distribution Using Counts-In-Cylinders. *The Astrophysical Journal*, 698(1):143–154, June 2009.
- [85] Martin White, M. Blanton, A. Bolton, D. Schlegel, J. Tinker, A. Berlind, L. da Costa, E. Kazin, Y. T. Lin, M. Maia, C. K. McBride, N. Padmanabhan, J. Parejko, W. Percival, F. Prada, B. Ramos, E. Sheldon, F. de Simoni, R. Skibba, D. Thomas, D. Wake, I. Zehavi, Z. Zheng, R. Nichol, Donald P. Schneider, Michael A. Strauss, B. A. Weaver, and David H. Weinberg. The Clustering of Massive Galaxies at $z \sim 0.5$ from the First Semester of BOSS Data. *The Astrophysical Journal*, 728(2):126, February 2011.
- [86] Surhud More, Hironao Miyatake, Rachel Mandelbaum, Masahiro Takada, David N. Spergel, Joel R. Brownstein, and Donald P. Schneider. The Weak Lensing Signal and the Clustering of BOSS Galaxies. II. Astrophysical and Cosmological Constraints. *The Astrophysical Journal*, 806(1):2, June 2015.
- [87] Chiaki Hikage and Kazuhiro Yamamoto. Impacts of satellite galaxies on the redshift-space distortions. *Journal of Cosmology and Astroparticle Physics*, 2013(8):019, August 2013.
- [88] Risa H. Wechsler, Andrew R. Zentner, James S. Bullock, Andrey V. Kravtsov, and Brandon Allgood. The Dependence of Halo Clustering on Halo Formation History, Concentration, and Occupation. *The Astrophysical Journal*, 652(1):71–84, Nov 2006.
- [89] Neal Dalal, Martin White, J. Richard Bond, and Alexander Shirokov. Halo Assembly Bias in Hierarchical Structure Formation. *The Astrophysical Journal*, 687(1):12–21, November 2008.
- [90] Yen-Ting Lin, Rachel Mandelbaum, Yun-Hsin Huang, Hung-Jin Huang, Neal Dalal, Benedikt Diemer, Hung-Yu Jian, and Andrey Kravtsov. On Detecting Halo Assembly Bias with Galaxy Populations. *The Astrophysical Journal*, 819(2):119, March 2016.
- [91] Boryana Hadzhiyska, Sownak Bose, Daniel Eisenstein, and Lars Hernquist. Extensions to models of the galaxy-halo connection. *Monthly Notices of the Royal Astronomical Society*, 501(2):1603–1620, February 2021.
- [92] Adam Paszke, Sam Gross, Francisco Massa, Adam Lerer, James Bradbury, Gregory Chanan, Trevor Killeen, Zeming Lin, Natalia Gimeshein, Luca Antiga, Alban Desmaison, Andreas Köpf, Edward Yang, Zach DeVito, Martin Raison, Alykhan Tejani, Sasank Chilamkurthy, Benoit Steiner, Lu Fang, Junjie Bai, and Soumith Chintala. Pytorch: An imperative style, high-performance deep learning library, 2019.
- [93] Roland de Putter, Olivier Doré, and Masahiro Takada. The Synergy between Weak Lensing and Galaxy Redshift Surveys. *arXiv e-prints*, page arXiv:1308.6070, August 2013.
- [94] ChangHoon Hahn, Roman Scoccimarro, Michael R. Blanton, Jeremy L. Tinker, and Sergio Rodríguez-Torres. The effect of fiber collisions on the galaxy power spectrum multipoles. *Monthly Notices of the Royal Astronomical Society*, page stx185, Jan 2017.
- [95] Hong Guo, Idit Zehavi, and Zheng Zheng. A new method to correct for fiber collisions in galaxy two-point statistics. *The Astrophysical Journal*, 756(2):127, Aug 2012.